Faculty of Science
University of Helsinki

Building the Future with Molecular Layer Deposition: Conductive, Insulating, and Thermally and Chemically Robust Polymeric Thin Films

Saba Rantanen
(née Ghafourisaleh)

ACADEMIC DISSERTATION
To be presented, with the permission of the Faculty of All Faculties of the University of Helsinki, for public examination in lecture room A129, Chemicum, University main building,
on 9th of May 2025, at 12:15.

Helsinki 2025

Thesis supervisor

Professor Mikko Ritala

Department of Chemistry

University of Helsinki

Helsinki, Finland

Preliminary examiners

Assistant Professor Tamar Segal-Peretz

Department of Chemical Engineering

Technion-Israel Institute of Technology

Haifa, Israel

Assistant Professor Matthias J. Young

Chemical Engineering

University of Missouri

Columbia, USA

Opponent

Professor Jukka Lukkari

Materials Chemistry of Sustainable Development

University of Turku

Turku, Finland

Publisher: Helsingin yliopisto
Series: Dissertationes Universitatis Helsingiensis 147/2025

ISBN 978-952-84-0886-4 (print)
ISBN 978-952-84-0885-7 (online)
ISSN 2954-2898 (print)
ISSN 2954-2952 (online)
PunaMusta, Joensuu 2025 Finland

“Nothing in life is to be feared, it is only to be understood. Now it is time to understand more, so that we may fear less.”

-Marie Curie

Abstract

In semiconductor technology, there has been a continuous drive to make devices smaller, more efficient, and more powerful. However, there are also challenges associated with the miniaturization. As individual components have to be smaller, it becomes harder to improve their performance. Researchers and engineers continuously work to address these challenges and push the boundaries of miniaturization. Precise thin film deposition methods, such as atomic layer deposition (ALD) and molecular layer deposition (MLD) can provide excellent control over film thickness and composition at nanoscale level.

Polymer thin films deposited by MLD offer unique properties for developing applications in energy and encapsulation of microchips, for example. These films can also perform as either conductive or insulating layers in electronics. Exploring novel MLD processes for polymer materials is crucial, especially when the aim is to achieve precise film thickness control with conformal coverage and uniform chemical composition.

In this thesis, I utilized combinations of organic monomers with inorganic reactants as oxidizer, linker and growth promoting co-reactant to deposit polymer thin films by the MLD method. The films showed thermally and chemically stable properties and were electrically either conductors or insulators.

Rhenium pentachloride ($ReCl_5$) was used as a strong oxidizer and EDOT (2,6-ethylenedioxythiophene) as an organic monomer for MLD of PEDOT thin films. The resulting PEDOT films exhibited highly desirable properties, namely high transparency and conductivity. I also developed thermally stable polybenzimidazole-like (PBI-like) and pyrrone thin films that demonstrated excellent chemical stability towards harsh acidic solutions and organic solvents. For the PBI-like films I used 3,3´-diaminobenzidine (DAB) and isophthalic acid (IPA) as the precursors. Trimethylaluminum (TMA) was used as a linker in the MLD process to facilitate condensation reactions between the acid and amine precursors. In addition, I deposited pyrrone films by utilizing DAB and pyromellitic dianhydride (PMDA) as the precursors and ozone as a growth promoting reactant.

The PBI-like and pyrrone films withstood elevated temperatures in air up to 400 and 300 °C, respectively, without significant degradation. This thermal stability is remarkable and valuable in applications where the materials must endure high-temperature conditions, such as thermal barriers, protective coatings, and high-temperature electronics.

Acknowledgements

The experimental work was carried out in the HelsinkiALD research group in the Department of Chemistry at University of Helsinki. European Union's Horizon 2020 research and innovation programme under the Marie Skłodowska Curie Grant Agreement No. 765378 is gratefully acknowledged for the financial support. ALD center Finland research infrastructure was used in the work.

My deepest gratitude is going to my supervisor, renowned Professor Mikko Ritala for his great guidance and support throughout these years. I was always feeling lucky and honoured to be part of your research group. This journey taught me more than I expected. Valuable life lessons were learned on this journey along with science and enjoyment of being with very nice people. You were always patient, and you gave me opportunities to explore and learn more. I have learned how it is important to be surrounded by patient, kind, supportive and humble people. Prof. Markku Leskelä and Prof. Matti Putkonen, thank you for your very calm, patient, and supportive attitude, I really appreciate your guidance and support throughout my research. You always advised me with insightful inputs which helped me a lot to find my way.

Dr. Marianna Kemell is acknowledged for her very kind and supportive guidance. I hadn't ever used a microscope of any kind before my Ph.D. studies. When you introduced me how to image surfaces of films, I was so excited to use the microscope and every time I was enjoying spending my time in the SEM room. It was so peaceful and at the same time exciting to image beautiful features. Thank you for your great work discipline and effort.

I had an opportunity to learn about ALD and MLD from scratch. I have learned so many valuable life lessons from my colleagues. They taught me how group work can improve work quality and how to be patient and wait to see that all hard work will pay off in the end. I would like to express my gratitude to Dr. Katja Väyrynen for her invaluable guidance and introduction to the field. Her commitment and diligent approach to work have truly inspired and left a lasting impression on me.

I want to thank Dr. Miika Mattinen for his great patience on explaining science concepts in a very fluent and understandable way. Dr. Miika, your great knowledge about everything was always highly appreciated and for me it was very enjoyable and pleasant to listen you. You were so kind that every time someone asked you something you patiently took your time to help people, I really appreciate your kind

and nice attitude. I want to thank Mikko Heikkilä for your friendly and kind approach even if you were very busy. You always tried to make some time for everyone to help. I really appreciate your support, Mikko; whenever I asked you to help me to measure or interpret XRD and XRR results you were there. I was so glad that we had someone like you to supervise us to work with the X-ray machine, which for me was very difficult to use, you were our expert to help us out.
Dr. Timo Hätänpää, Dr. Marko Vehkamäki, Dr. Elisa Atosuo, and Dr. Georgi Popov thank you for your very insightful thoughts and supportive guidance. You were always there whenever I had something to ask, and you explained everything patiently, so nicely and clearly. I would like to thank Dr. Chao Zhang for your friendly and nice attitude. You were a great lab company and I enjoyed chatting with you about our experiments and how we can make them work.
I would like to thank Dr. Kenichiro Mizohata for the most difficult quantitative polymer analysis. You were always explaining analysis results very nicely, thank you for your support. Dr. Peter King I really appreciate your great kindness and support to have an opportunity to work with a great team at Picosun and Applied Materials company and gain industrial work experience. Picosun company's Customer and Account Technology team is also acknowledged for the great support and encouragement.
Our memories won't be forgotten in room B343 with Dr. Heta Nieminen. We share a lot of memories, and I am so grateful that I had an opportunity to know you as a kind and very heartful person. I have collected so many nice memories with you. I would like also to thank Anton Vihervaara for his outstanding and cheerful personality. He is our team's youngest and loudest in a good way that always makes the coffee room vibe lively and loud. I had also the opportunity to know Dr. Alexander Weiss for his kind and friendly approach. He is so dedicated, polite and cheerful person. I would like to thank Dr. Ghazaleh Kia from the computer science department for her cheerful and positive characteristic. We first met each other in one of the Finnish courses and then continued to become very close friends. I won't forget our memories in Physicum, having sushi together and chatting about so many things.
My deepest appreciation extends to my parents and my brother that are always supportive, positive, and very kind. Without them it would not be possible even to think about my dreams. They are the great reason that I could reach where I always dreamed of. Finally, I want to express my heartful gratitude to my beloved husband Jaakko Rantanen, a great friend and dad of my son Kaarle Rantanen. I really appreciate your great support. You gave me the indescribable sense of having peaceful life. You thought me patience and calmness with your calm nature. Thank you, life got better with you, and I am looking forward to the future with you.

Saba Rantanen

List of abbreviations

3D	Three-dimensional
a.u.	Arbitrary unit
AFM	Atomic force microscopy
ALD	Atomic layer deposition
CVD	Chemical vapor deposition
DAB	3,3-diaminobenzidine
DMF	Dimethylformamide
EDOT	2,6-ethylenedioxythiophene
EDX	Energy-dispersive X-ray spectroscopy
FESEM	Field emission scanning electron microscopy
FTIR	Fourier-transform infrared spectroscopy
GIXRD	Grazing incidence X-ray diffraction
IPA	Isophthalic acid
ITO	Indium tin oxide
MOF	Metal-organic framework
MLD	Molecular layer deposition

PMDA	Pyromellitic dianhydride
SEM	Scanning electron microscopy
TG	Thermogravimetric analysis
TMA	Trimethylaluminum
UV-Vis	Ultraviolet-visible light
XPS	X-ray photoelectron spectroscopy
XRD	X-ray diffraction
XRR	X-ray reflectivity

Index

ABSTRACT **4**

ACKNOWLEDGEMENTS **5**

LIST OF ABBREVIATIONS **7**

LIST OF ORIGINAL PUBLICATIONS **11**

1 INTRODUCTION **12**

2 BACKGROUND **14**

2.1 Organic Thin Films 14

2.2 Hybrid Inorganic-Organic Materials 15

2.3 Solution Phase Deposition of Polymer Films 18

2.4 Vapor Phase Polymerisation Techniques 21

2.4.1 Chemical Vapor Deposition *23*

2.4.2 Molecular Layer Deposition *27*

2.4.3 Atomic and Molecular Layer Deposition of Hybrid Thin Films *31*

2.4.4 Physical Vapor Deposition *33*

2.5 Post Deposition Treatments 35

3 EXPERIMENTAL **38**

3.1 Film Deposition 38

3.2 Characterization Methods 39

4 RESULTS AND DISCUSSION **41**

4.1 Oxidative MLD of Poly(3,4-ethylenedioxythiophene) (PEDOT) Films 41

4.1.1 Film Structure and Composition *43*

4.2 MLD of Polybenzimidazole-Like (PBI-like) Thin Films 45

4.2.1 PBI-like Film Structure and Morphology *48*

4.2.2 PBI-like Film Nanostructures *50*

4.3 MLD of Polyimidazopyrrolone (Pyrrone) Thin Films 52

4.3.1 Pyrrone Film Growth *52*

4.4 Properties of the Films 56

4.4.1 Thermal Stability of PBI-like and Pyrrone *56*

4.4.2 Chemical Stability of PBI-like and Pyrrone Films *57*

4.4.3 Electrical and Optical Properties of MLD films *60*

5 CONCLUSIONS **64**

6 REFERENCES **66**

List of original publications

This thesis is based on the following publications:

I Ghafourisaleh, S., Popov, G., Leskelä, M., Putkonen, M., Ritala, M., Oxidative MLD of Conductive PEDOT Thin Films with EDOT and $ReCl_5$ as Precursors. *ACS Omega* **2021**, 6, 17545−17554.

II Ghafourisaleh, S., Hatanpää, T., Vihervaara, A., Mizohata, K., Vehkamäki, M., Leskelä, M., Putkonen, M., Ritala, M., Molecular Layer Deposition of Thermally Stable Polybenzimidazole-Like Thin Films and Nanostructures. *Adv. Mater. Interfaces* **2022**, 9, 2200370.

III Ghafourisaleh, S., Vehkamäki, M., Vihervaara, A., Zhang, C., Heikkilä, M. J., Leskelä, M., Putkonen, M., Ritala, M., Molecular Layer Deposition of Pyrrone Thin Films by Oxidative Polymerization. *Adv. Mater. Interfaces* **2023**,10, 2202174.

The publications are referred to in the text by their roman numerals.

I planned and executed the experimental work of the publications, wrote the first draft of the manuscripts, and finalized them with the co-authors. In publication II, T.H., A.V., and K.M. did the TGA, AFM, TOF-ERDA analysis of the PBI-like films respectively. M.H. did the GIXRD measurements of PEDOT films in publication I and the XRR and XRD measurements of pyrrone films in publication III. M.V. did the electrical measurements of the PBI-like and pyrrone films in publication II and III respectively.

1 Introduction

Polymeric thin films can be prepared with wet and dry processes.[1] Wet polymerization is done by casting or dipping substrate into a polymeric solution with methods such as Langmuir-Blodgett (LB)[2], electro-polymerization[3] and sol-gel[4]. Solution-based processes have however challenges in controlling film thickness and composition, especially when aiming for precise nanoscale applications. These limitations arise from factors such as solution homogeneity, reaction kinetics, and mass transport, which affect the uniformity and reproducibility of the resulting thin films.[5]

Miniature electronic devices with sophisticated features embed only a few nanometres or even sub nanometer thick layers of materials in their structures. In the case of polymer materials being of an interest in these devices, solution polymerization is not an option. Dry processes are needed for producing very thin layers of polymers for these applications.

Film depositions from gas phase, also known as dry processes, are done by either physical vapor deposition (PVD) or chemical vapor deposition (CVD).[1] In PVD solid source material is either evaporated or sputtered to form a thin film. In the CVD method[6] precursor vapors are introduced into a chamber simultaneously and they are chemically reacting and bonding onto a substrate surface. PVD is a milder method than CVD but in both cases continuous condensation of the source material onto the substrate makes it difficult to control the thickness and composition of the film.

To better control the thin film deposition in terms of film thickness and conformality, molecular layer deposition (MLD) has emerged as a technique that enables development of high-performance materials for energy-related, electronics and barrier applications. MLD thin films can be classified into two categories: organic and inorganic–organic hybrid materials. As compared to the inorganic thin films, organic films are flexible, light weight, and of low cost. MLD films are often highlighted for their thermal[7,8], chemical, and mechanical stability[9–11], and electrical[12],

optoelectronic[13–16], and thermoelectric[17–19] properties. Therefore, MLD is the best dry technique to deposit polymer and hybrid thin films.

The aim of this work was to study the possibility of depositing various MLD films and characterize their structural, compositional, thermal, chemical, and electrical properties. MLD of conductive PEDOT films, and thermally and chemically stable polybenzimidazole-like and pyrrone thin films with attractive electrical properties are shown for the first time in this work. The MLD processes explored in this thesis have led to a creation of films that make them ideal for a wide range of demanding applications, including electronics, energy devices, and protective coatings.

This thesis presents a literature review of common deposition methods for polymeric thin films. The basics of MLD are also introduced. The experimental part describes the MLD processes developed for the film deposition and the characterization methods used. The results on deposition and characterization of PEDOT, PBI-like and pyrrone thin films are then presented and discussed.[I–III]

2 Background

2.1 Organic Thin Films

Organic thin films serve a significant role in our daily lives. They find applications as light-transmitting coatings, optical control components in microelectronics such as optical sensors, and optical waveguides. Also, they have applications as detectors for sensing a wide range of organic, inorganic, and gas molecules in biosensors, and functioning as key materials in displays, electronic circuit elements, transistors, optoelectronic devices, and biochips.[20–22]

The emergence of organic semiconductors has paved the way for numerous electronic applications, thanks to their unique properties such as flexibility, transparency, cost-effective production, biocompatibility, and ecological sustainability due to the minimal energy consumption in their manufacturing processes. To date, the most notable achievements of organic semiconductor devices have occurred within optoelectronic devices, with a primary focus on displays based on organic light-emitting diodes (OLEDs). Organic solar cells (OSCs) also hold a great interest for building integrated photovoltaics, because of their lightweight and flexible nature, which facilitates straightforward installation of modules on rooftops and building facades.[23]

Conventional polymers like vinyl polymers, methacrylates, urethanes, and polyesters have traditionally been used in bulk applications. But apart from these polymers, the most prominent, and possibly the most promising candidates for thin-film devices are found in the realm of electro-optical devices utilizing conducting polymers such as polypyrrole and polyacetylene.

Conductive polymer materials are characterized by having conjugated double bonds within their chain structure, enabling electrons to be delocalized along the polymer chain. In highly conjugated polymer chains delocalized molecular orbitals of π-symmetry give rise to metal-like behavior. In order to make conductive polymer

materials through solution-based polymer processing, incorporation of side-chains or copolymer additives becomes essential.[22] Turning conductive polymers into thin films by solution methods depends on how well the polymer dissolves. The processes of casting and creating thin films through solution polymerization become complex when dealing with highly π-conjugated polymers. Conjugated polymers often exhibit elevated glass transition temperatures due to their rigid structures, preventing them from melting and rendering them insoluble in solvents. However, they have been made soluble through the introduction of suitable substituents, typically alkyl groups. Extensively studied polymers include polyanilines, polypyrroles, polythiophenes, polyfluorenes, and others (Scheme 1). These polymers have the ability to undergo physical or chemical transformations when subjected to heat, light, electric fields, or various chemical agents (dopants). These transformations result in diverse properties, including conductivity, fluorescence, reversible thermochromism, photochromism, electrochromism, and even ionochromism.[24]

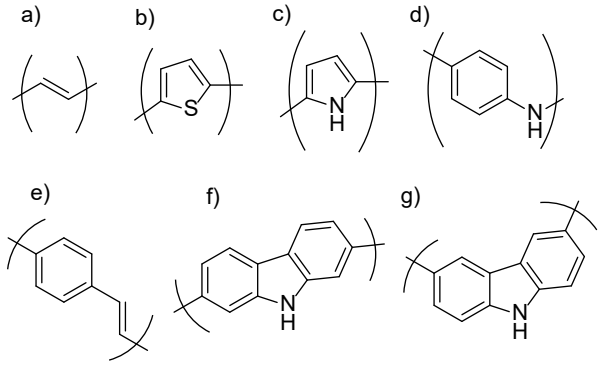

Scheme 1 Structures of conjugated polymers: (a) polyacetylene, (b) polythiophene, (c) polypyrrole, (d) polyaniline, (e) polyphenylene vinylene, (f) and (g) polycarbazole. Reproduced with permission, from Ref. [24]. Copyright 2013, John Wiley and Sons.

2.2 Hybrid Inorganic-Organic Materials

Hybrid materials have both organic and inorganic components in their molecular structures. Diversity of hybrid materials provides great potential for tailoring these materials for various applications ranging from energy storage and gas capture to sensing, catalysis, optics, and electronics. They can be used in applications like OLEDs (organic light-emitting diodes), OFETs (organic field-effect transistors),

semiconductors, fluorescent sensors, as well as within the scope of biological and medical applications.[25–28] Hybrid materials present significant potential for advancements in drug development, gene therapy, antibacterial agents, and tissue repair. Their unique properties enable innovative solutions in biological and medicinal fields, driving forward progress in healthcare and treatment methodologies.

Hybrid materials can be categorized into two groups based on the nature of the bonds connecting their inorganic and organic components. Group 1 features materials where these components are linked by weak Van der Waals, electrostatic, or hydrogen bonds. Group 2 consists of materials with strong covalent or ionic-covalent bonds between the constituents. Some hybrid materials exhibit both bond types but are primarily classified in group 2 due to the dominance of strong chemical bonds. These connections between organic and inorganic constituents give rise to functional materials with distinct properties. These properties are not solely determined by the sum of individual properties of each constituent but also arise from the profound synergy created by combining the constituents at the molecular level.[27,29]

Regardless of the bond type, various synthetic strategies exist for creating hybrid materials. As illustrated in the schematic view in Figure 1, hybrid materials are synthesized by four different paths.[27,29–35]

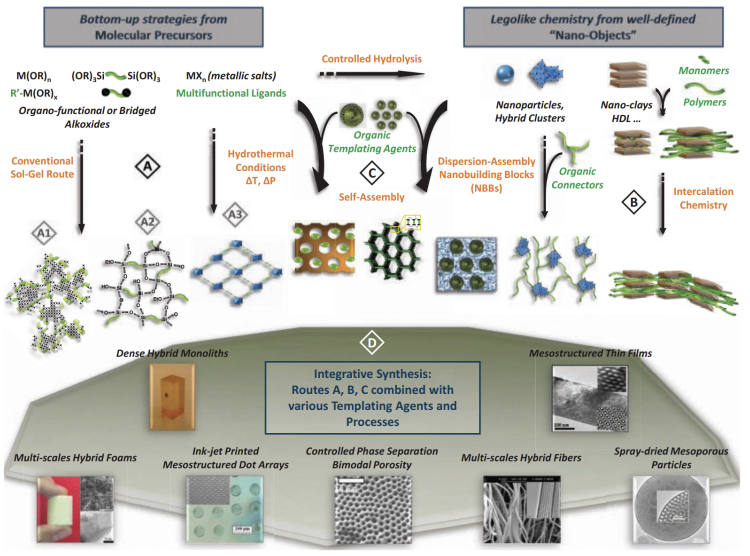

Figure 1 Scheme of the main chemical routes leading to nanostructured inorganic and hybrid organic/inorganic materials. (Reproduced with permission from Ref. [29], copyright 2010, Wiley).

Path A includes sol-gel as well as hydro/solvothermal synthesis, where molecular precursors such as metal alkoxides and metal salts together with complexing multifunctional and organofunctional precursors are used.

Path B consists of assembly of monodispersed nano-objects, including clusters and nanoparticles in the presence of organic molecules and polymers. Examples of clusters include metal oxides, metals and alloys, and chalcogenides. Path B also covers nanoparticle composites and nano-sheets of lamellar compounds such as clays, double hydroxides, phosphates, oxides, and lamellar chalcogenides.

Path C contains self-assembly of amphiphilic molecules (containing hydrophilic and hydrophobic functionalities) and polymers to generate supramolecular templates to control the texture and morphology of the growing inorganic solid or gel phase.

Path D is an integrative approach where the paths A, B and C are combined with templates of variable size (organo-gelifiers, bacteria, latex beads, submicron colloidal minerals) and physical chemistry of soft matter.

Metal-organic hybrid films are often referred as coordination polymers.[36] Organic ligands play an essential role in the construction of metal-organic coordination polymers (MOCPs), where their conformation, rigidity, and geometries have a significant impact on the resulting MOCPs. Rigid ligands can effectively dictate a precise geometry and alignment of metal clusters within the framework, enhancing the overall structural stability. These ligands often have functional groups, such as carboxylates, amines and pyridines, facilitating interactions with metal centers through coordination bonds. These interactions, in turn, determine the interconnectedness between the metal centers and ligands, thereby influencing the overall structure and stability of the framework.[28] Metal-organic frameworks, MOF, with crystalline and porous structures are a special type of MOCPs.[37–40]

As an example, for quite some time, the storage of hydrogen, a lightweight fuel, has posed significant challenges. While hydrogen holds promise as a clean energy source, storing it traditionally involves high-pressure compressed gas or extremely low temperature liquid. Both approaches raise concerns regarding safety during handling and refueling. Recognizing the limitations, researchers have turned to chemical storage alternatives.[41] An ongoing effort is the synthesis of hybrid and porous MOF structures that serve as viable energy storage materials for the hydrogen and other environmentally friendly fuels. In 2016, Rowsell and Yaghi synthesized $Zn_4O(C_8H_2O_4S_2)$ MOF framework also known as IRMOF-20.[41] As depicted in Figure

2, the structural arrangement of IRMOF-20 embeds two distinct cavity types with diameters of 17.3 and 14.0 Å. Notably, IRMOF-20 exhibited considerably improved performance in terms of surface area, pore sizes and diameters, as compared to the IRMOF-1,-2,-3 and-6, (prepared from benzene-1,4-dicarboxylic acid and its bromo-, amino-, and dihydrocyclobuta- derivatives, respectively). When these materials were tested for dihydrogen adsorption at – 196 °C IRMOF-20 exhibited the highest molar capacity. This outcome can be attributed to the larger surface area of organic adsorptive sites of thieno[3,2-b]thiophene units within the structure of IRMOF-20 and the favourable interaction between the framework and H_2 molecules (Figure 2).

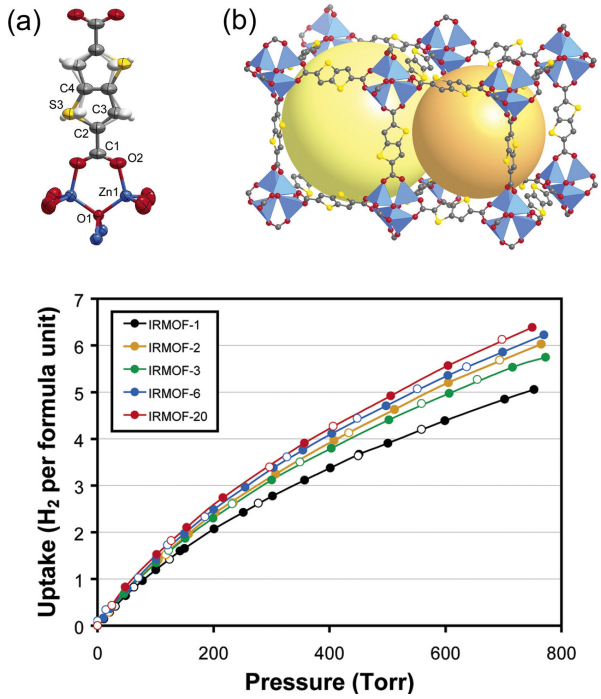

Figure 2 (a) A fragment of a crystal structures of the IRMOF-20. One orientation of the disordered link is shown in color, the alternate atomic positions of the other are shown in light gray. Atom colors: C dark gray, H white, O red, S orange, Zn blue. b) Two spherical pores of IRMOF-20 indicated as large yellow and orange spheres. The graph at the bottom shows dihydrogen adsorption curves determined at –196 °C as normalized per Zn4OL3 formula unit in a series of IRMOF-1,-2,-3,-6 and -20. Reproduced with permission, from Ref. [41]. Copyright 2006, American Chemical Society.

2.3 Solution Phase Deposition of Polymer Films

Solution phase deposition of polymers films stands out as a simple and economical technique, avoiding requirements for specialized vacuum chambers and intricate precursor delivery systems of vapor deposition methods. Polymer thin films can be deposited onto substrates from polymer solutions through processes such as Langmuir–Blodgett, self-assembly, layer-by-layer electrostatic deposition[24] (Figure 3), and spin-coating.[42]

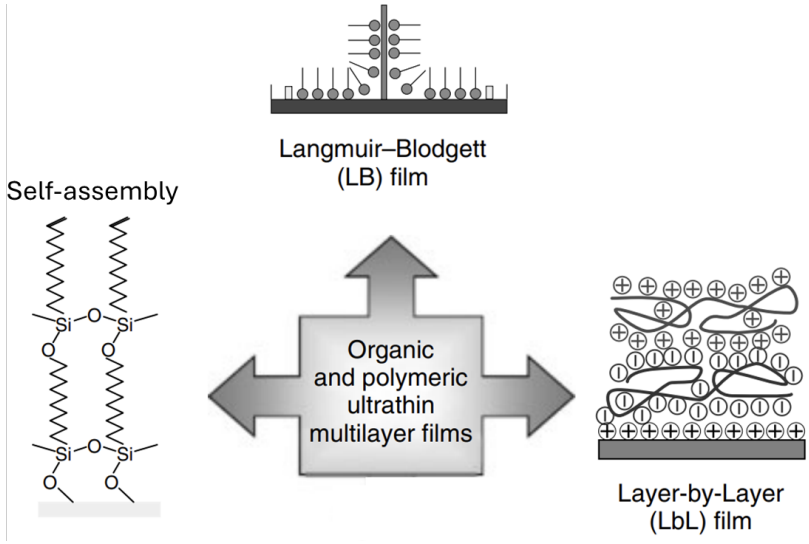

Figure 3 Ultrathin organic molecular and macromolecular deposition methods. Reproduced with permission, from Ref. [24]. Copyright © 2013 Wiley-VCH Verlag GmbH & Co. KGaA.

Langmuir films, also known as Langmuir monolayers, consist of amphiphilic molecules that are spread on the surface of a liquid, typically water. These molecules have a hydrophilic "head" region with an affinity for water, while their hydrophobic "tail" region orients toward the air phase. Langmuir-Blodgett (LB) films are created by transferring a Langmuir monolayer onto a solid substrate. To form multilayers, the substrate is alternately dipped into and withdrawn from the solution through the monolayer-covered surface of the solution.

Another category of organic thin films is self-assembled monolayers (SAMs), which are grown from either the gas phase or a solution. SAMs consist of organic molecules that arrange themselves into ordered domains on a surface. A typical SAM forming molecule includes three components: head, tail and functional end group. Head group interacts with the substrate and anchors the molecule. Tail group assembles away from the substrate. Functional end group is specific chemical functionality at the end of the

molecule. A defining characteristic of SAMs is the strong chemical interaction between the head groups of the molecules and the substrate.[43,44]

Common adsorbate-substrate pairs in SAMs include carboxylic acids on aluminum oxide or silver, alcohols, amines and isonitriles on platinum, and alkylsilane derivatives on hydroxylated surfaces. Additionally, dialkyl sulfides and disulfides are assembled on gold. Alkanethiols are assembled on metals like gold, silver, and copper, as well as on nonmetals such as GaAs, InP, and indium-tin oxide (ITO). Among these, alkanethiol-based SAMs on gold are extensively studied due to their reproducibility and well-defined structures.

In the layer-by-layer electrostatic deposition method, the driving force for building up multilayers is the ionic attraction between charges of the opposite polarity. The process begins with a solid substrate possessing a positively charged surface, which is immersed in a solution containing an anionic polyelectrolyte. This results in adsorption of a monolayer of the polyanion. Importantly, this adsorption occurs from relatively high concentrations of the polyelectrolyte, effectively reversing the surface charge. Subsequently, the substrate is rinsed with pure water, and then immersed in a solution containing a cationic polyelectrolyte. Here, another monolayer is adsorbed, restoring the original surface charge. When this process is repeated, multilayer assemblies composed of both polymers are formed.[42,44] This method has been applied for creation of layered structures involving partially doped polyaniline and a polyanion, such as sulphonated polystyrene. Additionally, it can be used to deposit biocompatible surfaces comprising alternating layers of charged polysaccharides and oppositely charged synthetic polymers, offering versatility in the design of functional materials for specific purposes. For example, these multilayer materials are used in applications for enhancing biocompatibility, tissue engineering and for controlled drug release.

Spin-coating is a widely adopted technique within the microelectronics industry for applying photoresist layers onto silicon wafers. The process starts by adding polymer solution onto the substrate wafer, which is then accelerated to a high-speed rotation, typically several thousand revolutions per minute. Alternatively, the solution can be added as the wafer slowly rotates. The spinning action causes the solution to spread radially outward, leading to a decrease in the thickness of the fluid layer. As the solvent evaporates from the solution, a uniform thin film is formed. The substrate surface may

be pre-treated with an adhesion promoter, such as hexamethyldisilazane (HMDS), to enhance wetting and promote better adhesion of the coating.[42]

While solution polymerization remains a widely adopted method with a long history of applications, its limitations within contemporary technology have prompted exploration and advancement of alternative approaches. The quest for dry, clean and cost-effective techniques has emerged as a response to the requirements of future material generations.

2.4 Vapor Phase Polymerisation Techniques

Vapor-phase polymerization (VPP) techniques represent clean and dry processes wherein monomers are evaporated or sublimed from a source to a reaction chamber. Subsequent chemical reactions take place on the surface of a solid substrate.[45–47]

The VPP method is similar to the processes used for depositing inorganic thin films, such as physical vapor deposition (PVD) and chemical vapor deposition (CVD). VPP deals with organic monomers and requires conditions tailored to their chemical nature.

VPP utilises either free radicals or ionic reactive species as initiators for the polymerisation reactions or condensation polymerisation without the use of initiators. Reactive species for the polymerization can be formed by low pressure plasmas, UV irradiation, oxidants and thermolysis of the monomer.[48]

VPP with oxidants is sometimes referred to as vapor deposition polymerisation (VDP). It is a two-step process (Figure 4). Initially, an oxidizing agent is deposited onto a substrate, followed by exposing the oxidant-coated substrate to monomer vapor within a sealed chamber, either at ambient pressure or under controlled low-pressure conditions. VDP involves oxidation polymerization of condensed monomers from the vapor phase onto the oxidant-coated substrate surface. This process leads to the synthesis and deposition of polymer films. Subsequently, the deposited film is washed with alcohol to eliminate any remaining unreacted oxidants, monomers and byproducts. Additionally, post-deposition treatment such as annealing may be conducted.[49]

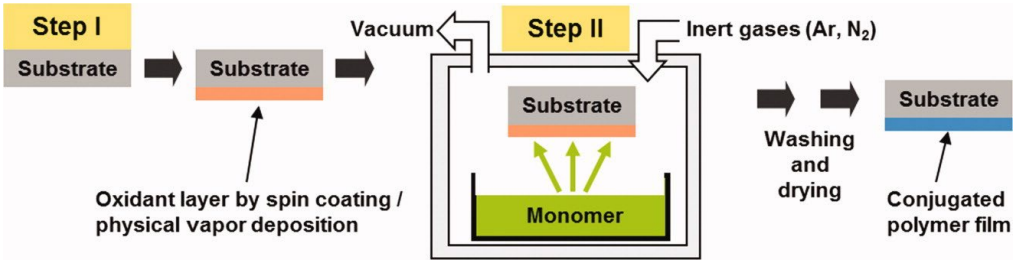

Figure 4 A typical procedure for a deposition of conjugated polymer films by VDP. Reproduced with permission from Ref. [49], Copyright 2012, Willey online library.

Figure 5 shows a schematic of a VPP chamber used for a deposition of PEDOT thin films. Fe(III)tosylate as an oxidant is deposited onto a substrate and acts as the polymerisation agent and, additionally, may also act as the dopant for the polymer. After placing the substrate into the chamber, EDOT monomer is evaporated in the chamber and the vapours are dispersed by a stirrer. Fe(III)tosylate facilitates the initiation of polymerization and removes electron from the EDOT monomer. This electron removal triggers the polymerization process, creating a highly conducting PEDOT film typically within 30 min.[46] Water vapor helps to regulate the process; a controlled level of humidity is essential for consistent polymer growth and prevention of the oxidant crystallization. Without proper water content, the oxidant may crystallize, leading to defects and poor film formation.

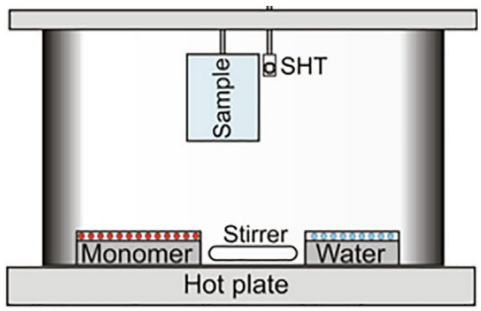

Figure 5 a) VPP chamber, as reproduced from Murphy and coworkers' work [46]. The oxidant-coated sample is suspended and a Sensirion humidity & temperature (SHT) sensor placed adjacent to the sample. Liquid EDOT monomer resides in a receptacle. Stirrer aids vapour dispersion. The VPP chamber resides on a hotplate; temperature is in the range of 60-70 °C. Reproduced with permission. Copyright 2010, Elsevier Ltd.

Polycondensation reactions in VPP[50,51] require monomers containing two or more reactive functional groups. These functional groups, such as hydroxyl, carboxyl, and

amino groups, condense to create longer polymer chains. The monomers are adsorbed from the vapor phase on the substrate surface, and when reactive chain ends of one monomer meet the chain ends of the co-monomer, they react to form an oligomer. The oligomers react further with the monomers or other oligomers, eventually forming a polymeric thin film on the substrate. VDP have been used to deposit a few polymers [49,52,53] as listed in Table 1. In the next chapter VPP techniques are categorized into CVD, MLD, and PVD based on their process conditions and precursor delivery system.

Table 1 Some of the polymer thin films deposited by VDP method.

Polymer	Linkage/repeating unit	Monomer	Oxidant
PEDOT	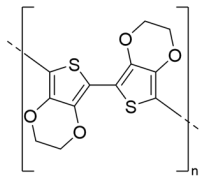	EDOT	$FeCl_3$
Polypyrrole	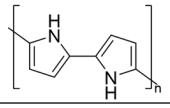	Pyrrole (Py)	$CuCl_2$, Fe(III) sulfonate or $FeCl_3$
Polyaniline	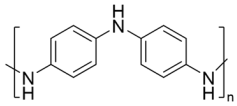	Aniline (PANI)	Fe(III) sulfonate, Ammonium peroxydisulfate
Polyhexylthiophene	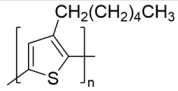	3-Hexythiophene (3HT)	$FeCl_3$

2.4.1 Chemical Vapor Deposition

In a CVD process evaporated monomers and other reactants are transported with a carrier gas into a reaction chamber and adsorbed on a heated substrate. In CVD chemical reactions take place between the precursor molecules and surface functional groups. CVD is a commonly used method for depositing inorganic thin films such as metals, alloys, and ceramics, and is valued for its robustness and cost-effectiveness. However, high processing temperatures can damage functional groups of polymers making it incompatible with polymer thin film deposition. Yet, modifications in CVD

reactants or reactor designs enable polymer deposition at lower temperatures, expanding the utility of this technique for polymer deposition.[6] By CVD it is possible to deposit highly crosslinked, insoluble polymers (poly(tetrafluoroethylene) (PTFE) and other fluoropolymers), copolymers of incompatible monomers (organic networks) and conducting polymers.[54]

CVD processes of polymers can be classified based on the polymerization mechanism, the activation method used to initiate the polymerization, the types of precursors used, or the system parameters involved. CVD of polymers is based on either chain-growth or step-growth polymerization mechanisms. In the chain-growth polymerization chains with free-radical species are successively added to form the polymer. Almost any chemical with vinyl group can be polymerized with this method. Poly(styrene), poly(methyl methacrylate) (PMMA) and low density poly(ethylene) are examples of the most common polymers formed using the free-radical chain-growth polymerization.

The chain-growth polymerization consists of initiation, propagation, and termination steps. In the initiation step free radicals are created by using an initiator such as light, heat or redox reaction. In the propagation step the polymer chains grow by the addition of monomer molecules to the free radical active sites. The termination step is the final step of the polymerization when the active sites of two chains, or the active site of a chain and a free radical meet and react which terminates the chain propagation.

One of the CVD techniques that is based on the chain-growth polymerization is plasma enhanced CVD (PECVD). In PECVD of polymers, plasma is used as the initiator of the process. Monomer molecules are bombarded with energetic plasma electrons, which leads to a breaking of bonds and creation of active monomer sites. Monomer molecules are attached to these active sites and transfer the radical group to the chain end where the polymerization continues. However, as the breaking of the monomer molecules by the electrons is an uncontrolled process, undesirable side reactions, such as dissociation, excessive crosslinking or fragmentation may occur. Plasma source generates radicals which are attacking chemical bonds and breaking down monomers to create energetic active radicals to cause side reactions. In these side reactions functional groups of the monomers can be damaged or destroyed leading to a loss of functionality. The ‘strength’ of the plasma on a specific monomer system can be quantified by the Yasuda parameter, which is defined as the ratio of plasma power (W)

to the flow rate of the monomer (F) times the molecular weight (M) of the monomer; W/FM. A low Yasuda parameter indicates gentle conditions, i.e. lower ion flux and less substrate heating.[55]

Partial retention of functional groups of monomers is possible also by using pulsed plasma. During the brief period when the plasma is on, ions and radicals are created, starting the initiation reactions. When the plasma is turned off, the propagation reactions dominate. Using the pulsed plasma methods, thin films of polymers such as PMMA[56] and fluorocarbons were formed with a partial retention of their functional groups.

Plasma enhanced CVD and pulsed-plasma CVD are widely employed techniques. However, when it comes to depositing polymer films through plasma, certain challenges arise. These include decreased polymerization rates resulting from an interplay between etching and deposition reactions. Both plasma methods lack selectivity which leads to unintended side reactions during the polymerization process.

Another type of CVD utilizing the chain-growth polymerization is initiated CVD (iCVD) where filaments are used as a heat source to thermally decompose initiator molecules required for the polymerization process. In iCVD, the monomer and initiator gases are introduced into the reaction chamber where the filament heats the initiator molecules, causing them to break down into free radicals. These free radicals then initiate the polymerization of the monomer on the substrate, resulting in the formation of polymer thin films. Chemical reactions in iCVD closely mirror traditional free-radical chemistry. An initiator is subjected to thermal decomposition, generating radicals that subsequently engage with vinyl monomers, facilitating the growth of polymer chains. Through this approach, a diverse selection of readily accessible vinyl monomers, particularly acrylates and methacrylates (Scheme 2) can be polymerised into thin films.

Scheme 2 Structures of a) acrylates and b) methacrylates monomers utilized in iCVD.

Polytetrafluoroethylene (PTFE, commonly known as Teflon) is another type of polymer thin film that can be polymerised by iCVD through thermal decomposition of

hexafluoropropylene oxide (HFPO) initiator.[57] Poly(dimethyl siloxane) (PDMS) and poly(oxymethylene) POM[58] are examples of thin films made by ring-opening iCVD polymerizations. For PDMS the polymerization is initiated by a thermal decomposition of a peroxide-based initiator, such as tert-butyl peroxide (TBP). These as initiators decompose to generate radicals that start the polymerization process, allowing the PDMS monomer to form thin films. Polymerization of POM typically uses organic peroxides or azo compounds as the initiators. These compounds decompose under heat to produce free radicals that trigger the polymerization of formaldehyde units into POM.

The range of polymers that can be deposited by iCVD is limited by the delivery of the precursors into the vacuum chamber and onto the substrate surface. The precursor molecules need to have a high enough vapor pressure to achieve a reasonable and steady flow rate into the reactor. iCVD utilizes selectively activated, thermally or photolytically labile initiators. This unique feature enables achievement of high deposition rates while ensuring the preservation of functional groups.

A variation of iCVD known as photo-initiated CVD (piCVD) involves simultaneous introduction of a photosensitive initiator along with a vinyl monomer into the chamber. In piCVD the photoinitiator is exposed to UV light, causing it to decompose and produce free radicals. For example, in sensor applications for biological systems the piCVD technique allows for the creation of biocompatible coatings and protective hydrogel thin films that ensure sensor stability and functionality in biological environments. UV light at a wavelength of 254 nm activates the polymerization of the HEMA (hydroxyethyl methacrylate) monomer, leading to the formation of hydrogel thin films on microspherical (small spherical particles) substrate without degrading response of the sensors. [59]

The method of oxidative CVD (oCVD)[60] enables the step growth of electrically conducting polymers such as poly(ethylenedioxythiophene) (PEDOT). In the earlier discussed VPP method, polymer thin films are deposited using predeposited oxidant in combination with vapor phase monomers. In oCVD, by contrast, a monomer and an oxidant are delivered to the substrate in a single step. Adsorption and spontaneous reaction proceed directly on the substrate. The oCVD method requires no hot filament, plasma or photoexcitation of the reactants, the process can be better controlled and is less aggressive than the processes that produce free radicals.[60]

As depicted in Figure 6a, the oCVD process entails loading of the oxidant into a crucible that is resistively heated. The substrate is positioned above the crucible. Through a side port, monomer vapor is introduced into the reactor where it spontaneously reacts with the oxidant, thereby commencing polymerization on the substrate surface. Figure 6b shows a chemical scheme of the polymerisation mechanism of PEDOT in oCVD.

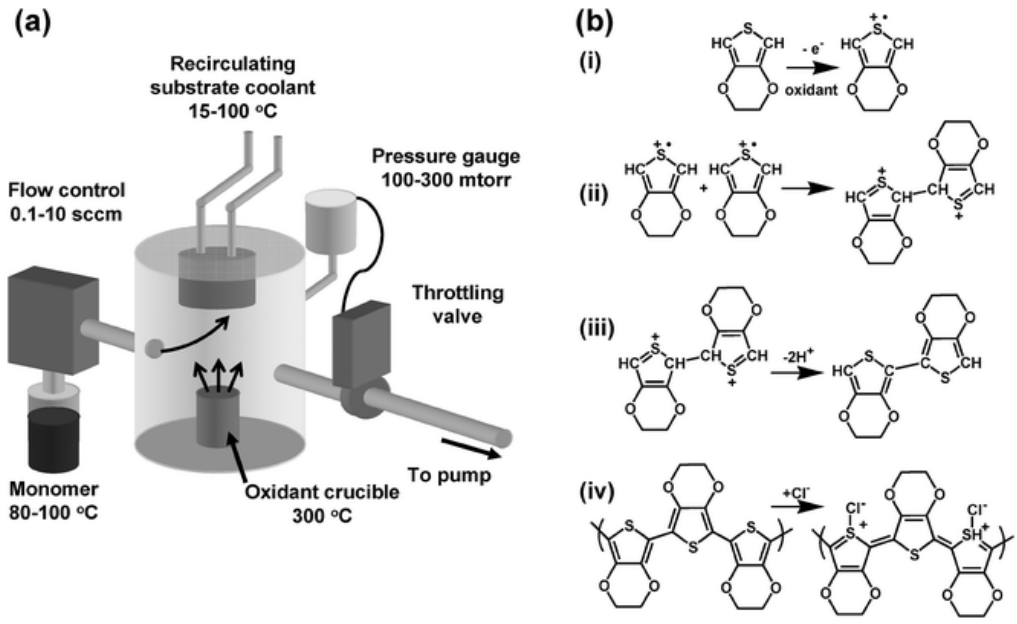

Figure 6 (a) Schematic of an oCVD reactor and typical operating parameters. (b) Chemical scheme of the oxidative polymerization of PEDOT. Reproduced with permission, from Ref. [60]. Copyright 2009, Royal Society of Chemistry.

2.4.2 Molecular Layer Deposition

MLD is a type of VPP where the reactant molecules are transported by a carrier gas to the reaction chamber alternately, one at a time, allowing the film to be grown layer by layer (Figure 7). MLD is used for deposition of organic and hybrid thin films from the gas phase onto solid surfaces. Similar to Atomic Layer Deposition (ALD) it operates through sequential pulses of precursors within a reaction chamber. Both ALD and MLD techniques enable film deposition on intricate 3D structures with high aspect ratios, primarily due to their inherently self-limiting nature.

In MLD, each precursor exposure leads to a self-limiting reaction, meaning that the reaction stops once all available reactive sites on the surface are occupied. This ensures

that only a monolayer of the precursor is deposited, regardless of the amount of precursor supplied. The self-limiting nature of MLD reactions ensures controlled film growth at the molecular scale. This is a critical feature, as it ensures uniform film growth across large, complex and high aspect ratio surfaces.

In the first half-cycle of MLD, precursor A chemisorbs and reacts with the reactive sites (e.g., hydroxyl groups) on the substrate surface. After a purge step with inert gas for removing the excess of the precursor A, in the second half-cycle, the precursor B reacts with the reactive sites created by the precursor A. This cycle is repeated to build a thicker film. The thickness of the resulting film is controlled by the number of MLD cycles repeated. In each cycle, the same amount of film is deposited, while excess precursor molecules and associated by-products are purged away, as depicted in Figure 7.

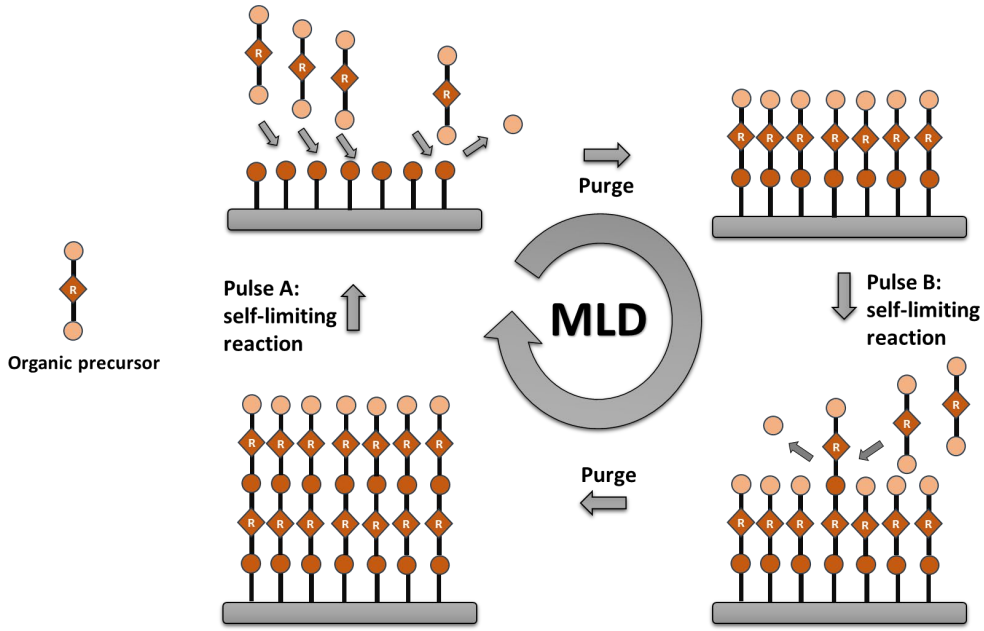

Figure 7 Schematic representation of one MLD cycle.

MLD was for the first time demonstrated in 1990's but has only recently started to attract more interest.[61] Materials library has expanded from polyimides and polyamides to other polymers. MLD is different from ALD because of using organic molecules as precursors. Most of the organic precursors have low volatility and high

source temperatures often increase the risk of precursor molecule decomposition. In MLD processes it is also common that the growth per cycle (GPC) decreases at elevated deposition temperatures.[62–66] At high temperatures organic molecules can easily desorb from the surface or decompose before reaching the substrate.

Saturation of GPC with increasing pulse length is characteristic of ideal ALD and MLD processes. However, generally in MLD processes no full saturation is reached due to the so-called "soft" saturation by non-self-limiting reactions of the reactants.[67–70] There are a couple of reasons that may affect the saturation in MLD processes. One is the choice of the precursor. Homobifunctional precursors[71] (same functional groups at both ends of the molecule) with long chains are prone to bend and make also a second bond to the surface (double reaction) which decreases the reaction sites available for the upcoming precursor molecules and thereby decreases the growth rate. Precursors with aromatic and rigid molecular structures are less likely to undergo double reactions with the surface than precursors with long and flexible molecular chains. Heterobifunctional precursors[72] (different functional groups at two ends of the molecule) avoid double reactions since only one functional group can make a bond with the reactive surface sites, while the other end of the molecule does not react with the surface.

Another reason for the non-saturative growth can be diffusion and absorption of precursor molecules inside the growing film. These molecules create additional reactive sites inside the film which may lead to an increase in the GPC. Despite the challenges, MLD is experiencing rapid growth for depositing thin films of various organic and hybrid materials.[65]

While condensation reactions dominate in MLD, there is an alternative of oxidative MLD (oMLD) where the film is grown through oxidative polymerization utilizing an oxidizing agent and an organic monomer. The concept behind oMLD,[49,52,73,74] originally developed for solution polymerization, was later adopted for vapor-phase deposition, evolving into techniques like oCVD and then oMLD. oMLD polymerization is a relatively new technique to deposit electrically conductive polymers for next-generation electronics, energy storage, photoresists, protective barriers, and other applications. Table 2 represents polymer thin films that have been deposited by MLD using either condensation or oxidation polymerisation reactions.

Table 2 Organic polymer films deposited by MLD, their linkage groups and precursors.

MLD (Condensation polymerisation)	Linkage/repeating unit	Organic monomers	
Polyamide[50]		Diamine and diacyl chloride	
Polyimide[66]	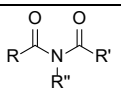	Diamine and acid dianhydride	
Polyurea[75]	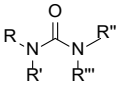	Diamine and diisocyanate	
Polyurethane[76]	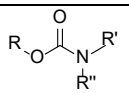	Diisocyanide and diol	
Polythiourea[77]	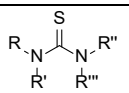	Diamine and diisocyanide	
Polyester[78]		Diachylchloride and diol	
Polyimine[79]		Diamine and dialdehyde	
poly(p-phenylene terephthalamide)[80]	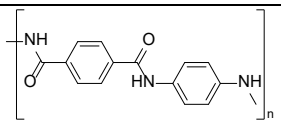	Terephthaloyl chloride and p-phenylenediamine	
oMLD (Oxidative polymerisation)	**Linkage/repeating unit**	**Organic monomers**	**Oxidants**
PEDOT [52,74,81]	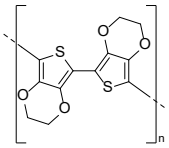	EDOT	$FeCl_3$, $MoCl_5$, $SbCl_5$, or $ReCl_5$
Polypyrrole[52,82]	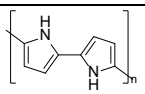	Pyrrole	$SbCl_5$ or $MoCl_5$
Polyaniline[52,82]	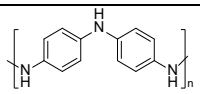	Aniline	$SbCl_5$ or $MoCl_5$
Polythiophene[52]	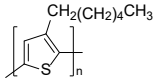	Thiophene	$SbCl_5$
Polyphenylenediamine[82]	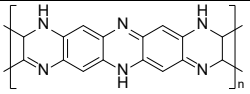	Phenylenediamine	$MoCl_5$

2.4.3 Atomic and Molecular Layer Deposition of Hybrid Thin Films

Research interest is increasing towards development of hybrid inorganic-organic thin films by ALD and MLD. Hybrid thin films have traditionally been deposited by using solution methods such as sol-gel, Langmuir–Blodgett, layer-by-layer, and electrochemical techniques.[25,83–85] These techniques do not provide precise thickness control and conformality on 3D structures. In addition, solution-based methods leave impurities in the film which prevent meeting requirements of many applications. As an alternative, combined ALD/MLD techniques[61] provide an efficient way to deposit inorganic-organic hybrid materials directly from gaseous precursors in a single process.[26,64,72,86–92]

Scheme 3 represents inorganic-organic hybrid thin film deposition by using inorganic and organic precursors. Hybrid thin films are formed by sequentially exposing the substrate to an inorganic precursor (ALD half cycle) and an organic precursor (MLD half cycle), separated by purge steps.

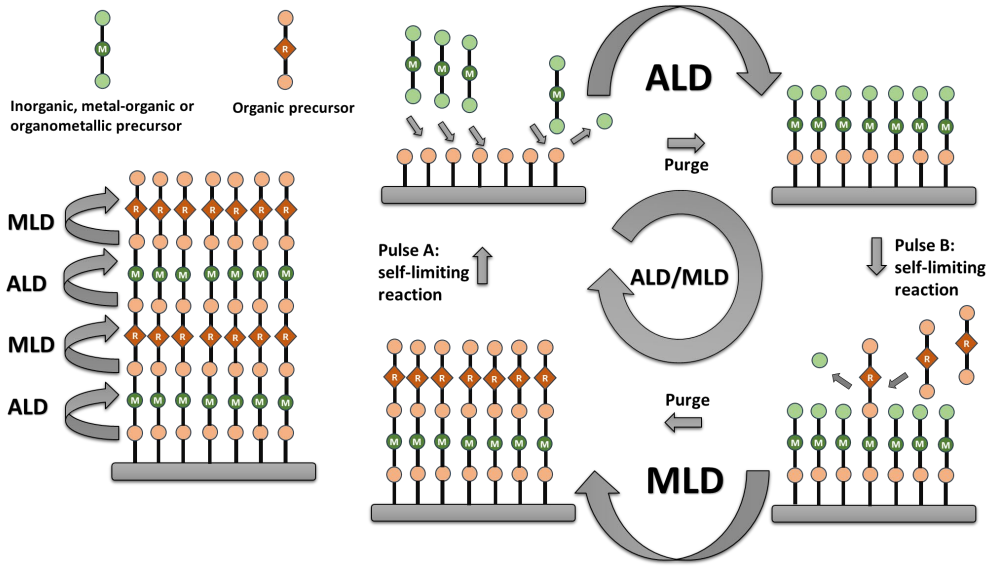

Scheme 3 Schematic representation of deposition of inorganic-organic hybrid thin film ALD and MLD using inorganic and organic precursors respectively.

Hybrid inorganic-organic thin films are often referred to as metalcones[65,93] when metal precursors are combined with alcohols or phenols. While a significant amount of research has centered around aluminum-based alucones, investigations have also

encompassed zincones, titanicones, and zircones.[26,64,65,71,72,86,87,89,91,92,94–98]

For example, in an alucone MLD process, TMA reacts with surface hydroxyl groups (-OH) to form aluminum methyl groups (-$AlCH_3$) on the surface. These methyl groups serve as reactive sites for the next precursor in the second half-cycle. Continuing with the alucone example, the second precursor can be ethylene glycol (EG, ethane-1,2-diol), which reacts with the surface -$AlCH_3$ groups to form an Al-O linkage, with the release of methane (CH_4) as a byproduct. This creates new -OH groups on the surface, resetting the surface for the next TMA pulse, and the process repeats.

In Figure 8, we see schematic representations of the ideal structures of hybrid films[65] formed from trimethylaluminum (TMA) + ethane-1,2-diol, diethylzinc (DEZ) + benzene-1,4-diol, and TMA + oxiran-2-ylmethanol. These examples illustrate the characteristic structures of these film types.

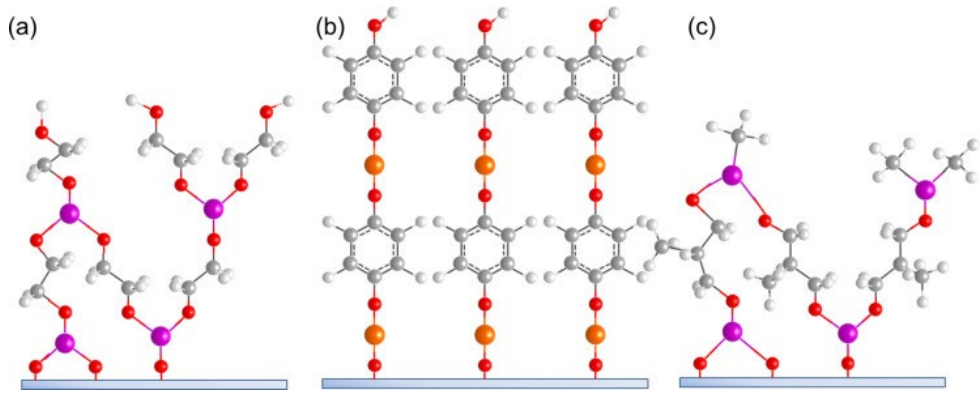

Figure 8 Schematic illustration of ALD/MLD inorganic–organic hybrid thin films deposited by using (a) TMA with ethane-1,2-diol, (b) DEZ with benzene-1,4-diol, and (c) TMA with oxiran- 2-ylmethanol. Reproduced with permission, from Ref. [65]. Copyright 2014, the Beilstein Journal of Nanotechnology.

Figure 9 presents a schematic diagram illustrating three-step ABC reaction sequence used for the MLD of an alucone film.[97] The sequence involves three reactants: TMA, ethanolamine (EA), and maleic anhydride (MA). In step A, TMA reacts with surface carboxylic groups (-COOH) to form surface-bound -$AlCH_3$ and releases methane as a byproduct. In step B, the surface-bound -$AlCH_3$ reacts with the hydroxyl group of EA, forming -Al-$OCH_2CH_2NH_2$ groups and releasing further methane. Finally, in step C, MA reacts with the amine group (-NH_2) on the surface to form new carboxylic acid

groups through a ring-opening reaction, completing the cycle and preparing the surface for the next sequence.

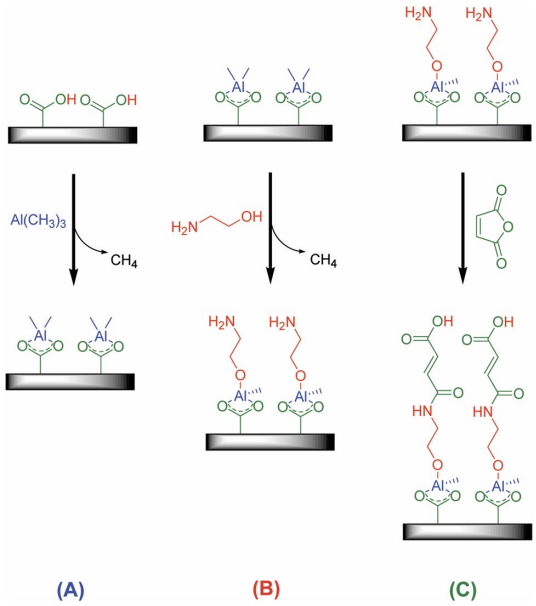

Figure 9 Schematic of three-step reaction sequence for ABC alucone growth using (A) trimethylaluminum (TMA), (B) ethanolamine (EA), and (C) maleic anhydride (MA). Reproduced with permission, from Ref. [97]. Copyright 2009, American Chemical Society.

2.4.4 Physical Vapor Deposition

PVD is conducted within a vacuum environment (Figure 10). It involves either evaporating a solid or molten source (Figure 10b) or utilizing energetic ions from a plasma to sputter atoms or molecules from a source target (Figure 10a).[99–104] The evaporated or sputtered atoms or molecules subsequently travel through the vacuum and condense onto the substrate, forming the desired film. There are three common methods for evaporating materials: electron-beam (e-beam) heating, resistance-heating, and RF induction-heating.[2,105]

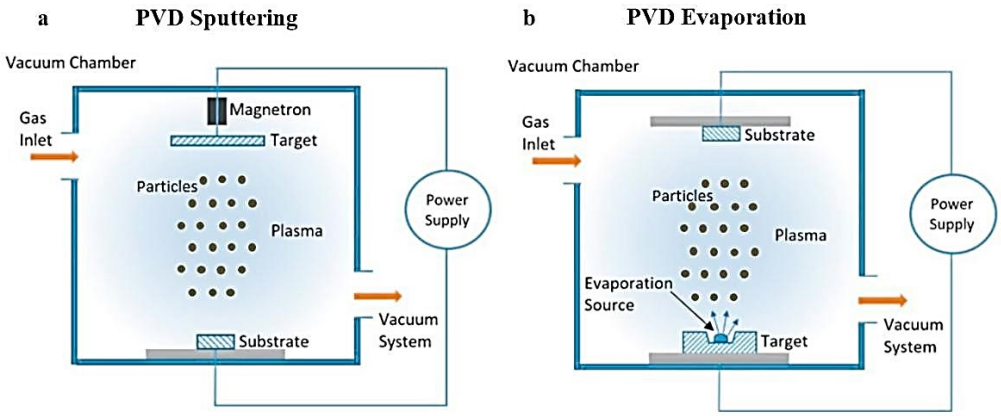

Figure 10 Schematic diagrams of the a) sputtering and b) evaporation methods. Reproduced with permission, from Ref. [105]. Copyright 2018, Elsevier.

There have been attempts to deposit polymer films, especially fluoropolymers by the sputtering method.[99,102] Upon ion bombardment, a polymer target emits volatile fragments into the plasma instead of the polymer molecules in evaporation. The sputtered small molecular fragments serve as a monomer gas. The fragments recombine and produce a thin film by a mechanism similar to the plasma polymerization. Consequently, polymer films deposited by the sputtering method have similar characteristics to those deposited by plasma polymerization.[100,103]

Plasma polymerisation and sputtering methods both involve complicated collisions between molecules and electrons, generating various ionic and radical species due to the glow discharges used in the processes. These methods are suitable for producing polymers with robust networks but are unable to control molecular structure precisely to form high-molecular weight (high-MW) polymers.

There are only a few polymers that can be directly evaporated into the vacuum chamber to form a film. For the direct evaporation polymers are required to have low molecular weight and weak intermolecular interactions such as polyethylene (PE) which is a typical example of a polymer that can be directly evaporated into the vacuum chamber. Other polymers that have been deposited by direct evaporation are poly(vinylidene fluoride) and polytetrafluoroethylene (PTFE) or Teflon.[24]

The fundamental characteristic that sets PVD methods apart is that the film deposition onto the substrate occurs in a line-of-sight manner. The film is deposited only on those areas of the substrate that are directly in the line of sight from the source. Therefore, the films have poor conformality.

2.5 Post Deposition Treatments

Post deposition treatments are often used to enhance structural, electrical, thermoelectrical and optical properties of thin film materials [106–108] to provide a higher degree of control over the final film characteristics. Post deposition treatments enable fine-tuning of structural properties of the films to meet the specific requirements of different device applications, ultimately leading to better performance and functionality. Post deposition treatments are crucial for tailoring structures and properties of polymer thin films in organic electronics. Eventually, post deposition treatments allow for modification of film morphology and molecular orientation, which are vital for enhancing performance of devices such as transistors and solar cells.[109]

There are several methods and motivations for the post deposition treatments such as annealing to densify atomic and molecular structures, and solvent treatment to change molecular orientation of polymers on a surface[107,110] to optimise photocatalytic activities[65] and enhance electrical conductivity. Thermal annealing increases crystallinity of polymer films, enhancing their charge transport properties and decreasing trap densities, which are beneficial for the efficiency and stability of devices. Solvent-vapor annealing method helps to control grain size and improve molecular packing, further enhancing the electrical properties of the films. Exposure of polymers to proper solvent vapors allows for the control of crystallization kinetics and nucleation density of monomers, resulting in a more desirable film morphology by dissolving and recrystallizing the polymer chains. Some examples of polymer thin films that have been post treated to enhance their properties for various applications will next be introduced.

Hexabenzocoronene (HBC) films[111] can be crystallized through hexane-vapor thermal annealing and applying PDMS (polydimethylsiloxane) stamp in a direct contact with the HBC films. These post deposition treatments result in films with a well-defined out-of-plane orientation that enhances charge transport properties. Poly(3-hexylthiophene) (P_3HT) thin films[112] have been thermally annealed to improve their crystallinity and molecular ordering. This process enhances the performance of organic thin-film transistors and solar cells by optimizing charge carrier mobility and light absorption characteristics.

Poly(3,4-ethylenedioxy-thiophene):poly(styrenesulfonic acid) (PEDOT:PSS) is another example of a conductive polymer thin film for which post deposition treatments have been studied extensively to improve the conductivity.[58,113–116] These methods have used heat, light, organic solvent, ionic liquid, surfactant, and acid or alkali treatments.

PEDOT has been the most conductive polymer, and it is known for its poor thermal conductivity and good electrical conductivity. Increasing the electrical conductivity of PEDOT would make it a suitable material for thermoelectric applications. Thermoelectric materials convert heat to electrical energy. There is a recent review by Joherul et. al[117] that lists solvent and acid post deposition treatment methods that have been used to enhance the electrical conductivity of PEDOT (Table 3).

Table 3 Summary of some of the reported solvent and acid post-treatment methods for enhancement of the electrical conductivity of PEDOT: PSS.

Acid and solvent post-treatment methods	σ_{max} **(S cm^{-1})**	
	No treatment	**Treated**
H_2SO_4[118]	0.3	3065
H_2SO_4[119]	0.2	4380
H_2SO_4[120]	0.8	2600
Triflic acid (TFSA)[121]	0.7	2980
H_2SO_4[122]	7	3000
H_2SO_4[123]	0.8	2673
H_2SO_4[124]	4.2	6323
HBr-DMSO [125]	0.4	1813
Camphor sulphonic acid (CSA) [126]	1.5	1826

As an example, Khasim et. al[126] in 2022 reported deposition of highly conductive, flexible, and transparent PEDOT:PSS films doped with dimethylformamide (DMF) followed by post treatment with camphor sulphonic acid (CSA). The post-deposition treatment significantly enhanced the conductivity of the PEDOT-PSS films from 1.5 S

cm^{-1} to 1826 S cm^{-1}. The post-treated PEDOT-PSS film on a polyethylene terephthalate (PET) substrate showed excellent transmittance (~87%) in the wavelength range of 400–800 nm. They fabricated flexible polymer electrodes with excellent electrical, optical, and electrochemical properties for possible optoelectronic and energy storage applications (Figure 11).

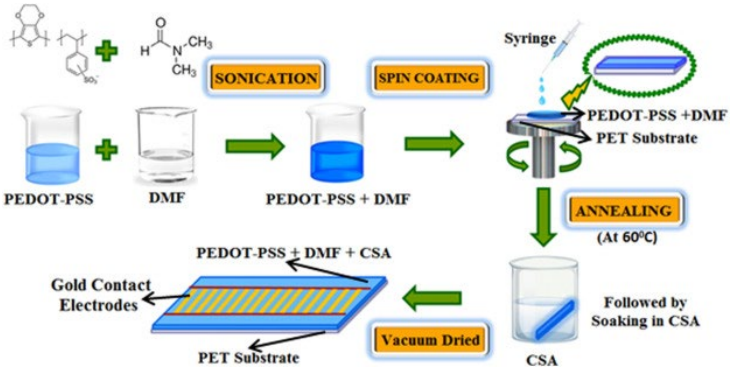

Figure 11 Fabrication of a flexible electrode from a PEDOT-PSS:DMF film deposited by spin coating and post treated with CSA. Reproduced with permission, from Ref. [126]. Copyright@2022, Elsevier B.V.

3 Experimental

3.1 Film Deposition

All films were deposited in a hot-wall, flow-type ASM Microchemistry F-120 ALD reactor. Nitrogen (N_2, AGA, 99.999%) was used as the carrier and purging gas and the pressure inside the reactor was ~2 mbar. The substrates were silicon (100), soda lime glass and ITO films on glass. All the precursors used in this thesis and their evaporation/sublimation temperatures, suppliers, and purities are listed in Table 4. Water, TMA, and bromine were pulsed into the reactor from external sources through needle and solenoid valves at room temperature.

Table 4 All the precursors used in this thesis.

Precursor	Evaporation/Sublimation Temperature(°C)	Supplier, Purity
2,6-Ethylenedioxythiophene, EDOT (I)	35–45	TCI, 95–98 %
Rhenium pentachloride, $ReCl_5$ (I)	110–115	Strem chemicals, IMC, 99.9 %−Re
Antimony pentachloride, $SbCl_5$ (I)	25–30	abcr chemicals, 99 %
Vanadium trioxychloride, $VOCl_3$ (I)	RT	abcr chemicals, ≥99 %
Bromine, Br_2 (I)	RT	ACROS organics, >90 %
Isophthalic acid, IPA (II)	60–165	TCI, >99.0 %
3,3´-Diaminobenzidine, DAB (II), (III)	210–220	Merck, ≥98 %
Pyromellitic dianhydride, PMDA (III)	145–160	TCI Europe Research Chemicals, >98.0 %
Trimethyaluminium,TMA (II)	RT	Volatec Ltd., 97%

3.2 Characterization Methods

Film thicknesses were measured with a Film Sense FS-1 Multiwavelength ellipsometer with the Cauchy on Si optical model.[I-III] Transmission spectra were measured using a UV/Vis spectrophotometer (Hitachi U-2000).[I-III] Crystallinity of PEDOT films was studied with X-ray diffraction (XRD) using a PANalytical X'Pert Pro MPD diffractometer.[I]

Morphology of the films was studied with a Hitachi S-4800 FESEM, and with a Veeco AFM.[II-III] The AFM measurements were performed in air by using Si probes with a tip radius of 10 nm, a spring constant of 40 N m^{-1} (Model: RTESP-300 from Bruker). Oscillation frequency of 250– 300 kHz was used and optimized within this range for each individual measurement. The images were flattened to remove artifacts from sample tilt and scanner bow, and the roughness was calculated as a root-mean-square value (Rq). Infrared spectra (Bruker Optics) with a 4 cm^{-1} spectral resolution were measured to get information about the chemical bonding between the atoms in the films.[II-III]

The composition of the PBI-like films was analyzed by TOF-ERDA with a 5 MV tandem accelerator EGP-10-II. A 35 MeV 79 Br^{7+} ion beam was used, and the measurement geometry was 20° + 20° (40° scattering angle).[II]

Resistances of PEDOT thin films deposited on glass substrates were measured at room temperature using a four-point probe instrument (CPS Probe Station, Cascade Micro tech combined with Keithley 2400). The as-deposited samples were stored in a desiccator prior to the measurement in order to minimize their exposure to the ambient air. For electrical measurements of the insulating PBI-like and pyrrone films, capacitors were made from the films as a dielectric and ITO and Al films as the electrodes. The polymer films were deposited on the ITO films on glass and Al electrodes were patterned on top by evaporating aluminum through a shadow mask by an Electron Beam Evaporator IM9912. A contact to the bottom ITO electrode was made in the corner of the sample by scratching through the film and soldering a wire. The capacitance C of the film was measured with a HP 4284A Precision LCR meter from Hewlett Packard. From the measured capacitance the dielectric constant ε_r (also called as k) was calculated as

$$\varepsilon_r = C \times d/\varepsilon_o \times A \quad (9)$$

where d is the thickness of the film, ε_o is the dielectric constant of vacuum, and A is the area of the top Al electrode (2.04×10^{-7} m^2). Leakage current measurements were carried out by a Keithley 2450 Source Meter (Keithley Instruments, Cleveland, OH, USA).[II-III]

Electroblowing of polyvinylpyrrolidone fibers

Precursor solution for the electroblowing was made from PVP, $(C_6H_9NO)_n$, M.W. 1 300 000, Alfa Aesar) and ethanol (96 vol%, GPR RECTAPUR). For preparing PVP fibers on Si substrates a 12 wt% of PVP/EtOH solution was electroblown into fibers by using a self-made equipment.[127]

Thermogravimetric analysis of PBI-like film

TGA of the as prepared and MLD coated electroblown PVP fibers were conducted with a NETZSCH STA 449 F3 Jupiter system. All measurements were conducted in both flowing air (20 mL min^{-1} air/20 mL min^{-1} N_2) and nitrogen (20 mL min^{-1} N_2/20 mL min^{-1} N_2) atmospheres. In isothermal measurements the samples were heated with a rate of 10 °C min^{-1} from 25 to 450 °C and then kept at 450 °C for 2 h. Dynamic measurements were conducted with a heating rate of 20 °C min^{-1} in a temperature range of 25–800 °C for the bare PVP fibers and 25–1000 °C for the PVP fibers coated with the PBI-like film.[II]

Chemical stability of PBI-like and pyrrone films

Chemical stability of the films deposited on silicon substrates was tested by immersing the samples into different concentrations of strong acid solutions for 24 h.[II-III] Hydrochloric acid (37%, British Drug Houses (BDH)), sulfuric acid (98%, BDH), phosphoric acid (97%, BDH), and formic acid (98%, BDH) were used for the chemical stability tests. Solubility of the PBI-like and pyrrone films into different organic solvents was also examined. These solvents were ethanol (96%, BDH), acetone (≥99.5%, Honeywell Riedel-de Haën), dimethylsulfoxide (≥99.5%, Honeywell Riedel-de Haën), and isopropyl alcohol (≥99.5%, Honeywell Riedel-de Haën).[II-III]

4 Results and Discussion

The main results of this thesis are summarized in this chapter. A more detailed description of the processes and characteristics of the films can be found in publications I–III.

4.1 Oxidative MLD of Poly(3,4-ethylenedioxythiophene) (PEDOT) Films

PEDOT polymer is highly valued for its excellent electrical conductivity, transparency and flexibility, making it ideal for a wide range of electronic applications such as flexible displays, solar cells, and sensors. Main motivation in publication I was to introduce and test $ReCl_5$ as a new oxidizing agent to polymerise EDOT monomers. Due to its high thermal stability and strong oxidizing ability $ReCl_5$ is a suitable candidate for this process. Additionally, $ReCl_5$ is structurally and chemically similar to $MoCl_5$ which has been traditionally used as an oxidant in similar processes. This similarity includes comparable reduction capability, which is essential for the efficient oxidation of the EDOT monomers as necessary for the PEDOT film formation.

PEDOT films were deposited by oMLD by pulsing alternately EDOT monomer and $ReCl_5$ as an oxidant at a temperature of 200°C which resulted in deposition of conductive films. The oxidant has an important role in polymerization of the EDOT monomer. In addition to $ReCl_5$, other oxidizing agents such as Br_2, $SbCl_5$, $VOCl_3$, and O_3 were tested. Among the oxidants tested, $ReCl_5$ was notably effective as a strong oxidant, facilitating the polymerization process. On the surfaces of the films, distinctive particulates containing rhenium and chlorine, originating from $ReCl_5$, were observed. These particulates were soluble in water, whereas PEDOT is insoluble in water. The films could be easily cleansed of the particulates by rinsing them with deionized water at a temperature of 25°C. Subsequently, the films were

subjected to detailed characterization both before and after the water rinse post-treatment.

The deposition of PEDOT thin films occurred at temperatures ranging from 125 to 200°C. At temperatures exceeding 200°C, no film deposition was achieved, while at lower temperatures the films exhibited undesirable properties, such as being flaky, nonuniform, and having an opaque black appearance. Therefore, 200°C was the optimum temperature to deposit PEDOT with this process.

With both precursors, EDOT and $ReCl_5$, no complete saturation of the growth rate was observed at 200°C (Figure 12). However, upon evaluating the growth rates from the rinsed thin films, improved saturation became evident. The growth rate maintained a relatively constant value of around 0.5 Å per cycle when either the $ReCl_5$ or EDOT pulse times were extended (Figure 12). Thicknesses of the films were increasing with increasing the pulse lengths of the $ReCl_5$ and EDOT precursors when measured before the water rinsing post-treatment. With the water rinsing major part of impurities were removed and the saturation seemed to have been achieved with already 0.5 s pulse length for both the $ReCl_5$ and EDOT precursors.

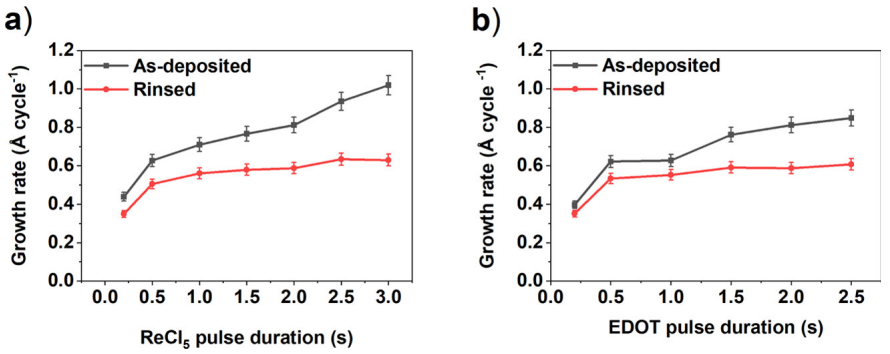

Figure 12 Growth rates of the films deposited at 200 °C by varying the pulsing durations of (a) $ReCl_5$ and (b) EDOT.

Number of particulates on the surfaces of the as-deposited films increases when the $ReCl_5$ pulse time is extended (Figure 13a). This increase contributes to the non-saturating growth observed with the films as-deposited, a trend that becomes more apparent with increased precursor pulse times as the particulates accumulate on the surface and affect the film thickness measured by an ellipsometer and thereby

also the growth rate (Figure 12). However, by the water rinsing, the particulates were successfully eliminated from the film surfaces. (Figure 13b)

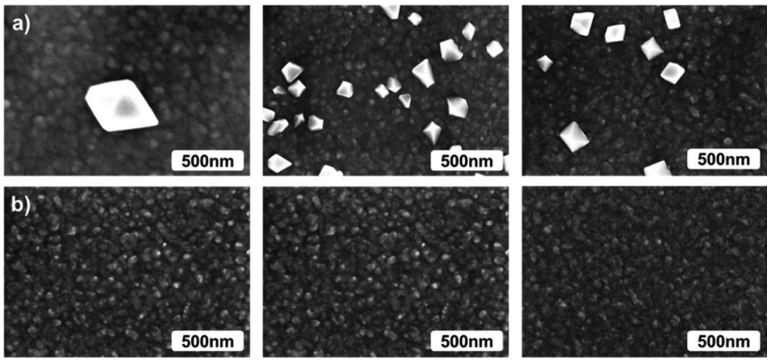

Figure 13 SEM images of a) as-deposited and b) water-rinsed PEDOT films deposited with 1000 cycles at 200 °C using, from left to right, 0.2, 0.5, and 1.0 s pulses of $ReCl_5$.

4.1.1 Film Structure and Composition

The PEDOT films obtained with relatively short $ReCl_5$ pulses of 0.2, 0.5, and 1.0 seconds exhibited in GIXRD reflections that correlated with the ReO_3 crystal structure (Figure 14a). These peaks disappeared after the films were rinsed with water, indicating that ReO_3 was present in the particles that were eliminated by the water rinsing (Figure 14b).

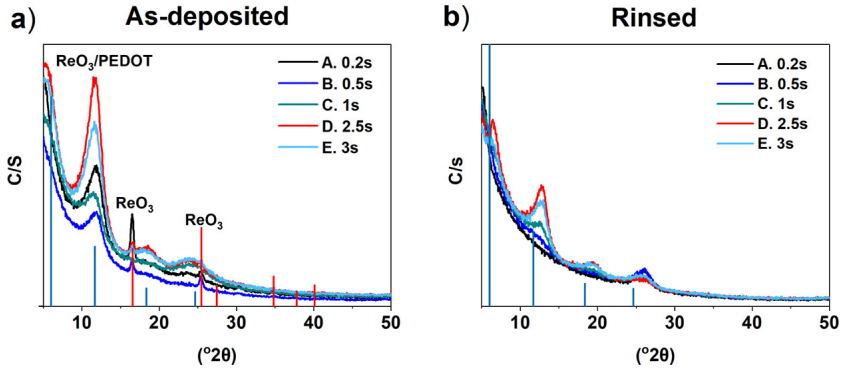

Figure 14 GIXRD reflection patterns of PEDOT films on Si. The films were deposited at 200 °C with 1000 cycles. (a) As-deposited. (b) After the water rinsing. The bars indicate positions of reflections measured from spin casted PEDOT films (blue bars).[128] Red bars indicate reflections of the ReO_3 [129] structure.

Thorough compositional investigations utilizing X-ray photoelectron spectroscopy (XPS) provided detailed insights into the film composition. As illustrated in Figure 15, XPS confirmed the presence of carbon, sulfur, and oxygen within the examined samples. The carbon 1s spectrum shows an intense peak at 284.7–285.0 eV, which is stronger than expected for PEDOT that has two peaks at 285.0 eV and 286.1 eV. The intense peak at 284.7–285.0 eV is ascribed to hydrocarbon contamination. This contamination likely also contributes to the shoulders observed at 287.0–289.0 eV, associated with carbonyl groups. The sulfur 2p spectrum displays a doublet at 163.5 eV ($2p_{3/2}$) and 164.7 eV ($2p_{1/2}$), consistent with the PEDOT structure. The main oxygen O 1s peak at 533.6 eV is characteristic of PEDOT, while a shoulder at 531.0 eV suggests a presence of hydroxide impurities. A distinctive O 1s peak at 528.3 eV, seen in the as-deposited film, is attributed to rhenium oxide, which is effectively removed after water rinsing, as indicated by its absence in the rinsed sample. Water rinsing decreased the rhenium content from 1.6 at.% to 0.5 at.% as compared to approximately 6 at.% Mo in the films deposited by MLD using $MoCl_5$.[81] In the as-deposited films, rhenium 4f lines indicated multiple oxidation states (II, VI, and VII). After the water rinsing, rhenium had mainly IV and VII oxidation states, with $ReCl_x$ and $ReOCl_x$ identified. Chlorine was not detected in either the as-deposited or water-rinsed films, though minor amounts might still influence the rhenium peak positions (Figure 15d). These findings highlight the impact of water rinsing on removing contaminants and decreasing the unwanted rhenium content, thereby refining the film purity and composition.

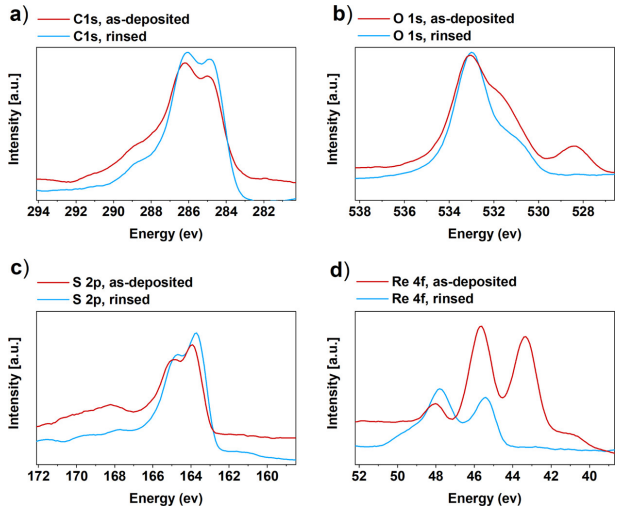

Figure 15 XPS results measured from the as-deposited and water-rinsed PEDOT films. (a) Carbon 1s, (b) oxygen 1s, (c) sulfur 2p and (d) rhenium 4f.

4.2 MLD of Polybenzimidazole-Like (PBI-like) Thin Films

PBI polymers are well known for their exceptional thermal stability, chemical resistance and mechanical strength, making them ideal for demanding applications such as fuel cells, membranes, and high-temperature coatings. In publication II the main objective was to introduce PBI thin film deposition and study electrical properties and thermal and chemical stabilities of the films. It is worth noting that the thin films deposited in publication II are referred as PBI-like films due to the presence of aluminium linkers in their composition.

The deposition of PBI-like thin films via MLD was done with isophthalic acid (IPA) and 3,3′-diaminobenzidine (DAB) as monomers, alongside with trimethylaluminum (TMA) as a linker precursor (Scheme 5). To achieve the growth of PBI-like structures with a reasonably high GPC, 225–280°C temperature range was utilized in this MLD process. Specifically, a temperature of 250°C was selected for depositing the PBI-like films, aiming to facilitate robust condensation reactions between the precursors. TMA was used as a linker in the deposition of the PBI-like films to promote the growth and enable formation of stable films. Without TMA, film growth did not occur due to weak adsorption or low reactivity of the monomers. Two distinct precursor pulsing sequences were tested: the ABCB sequence (TMA +

IPA + DAB + IPA) and the ABC sequence (TMA + IPA + DAB). These sequences yielded different types of PBI-like films. Notably, employing the ABCB sequence led to a GPC of 6.0 Å in the temperature range of 225–280°C, whereas the ABC sequence resulted in a GPC of 7.0 Å.

Previous study has demonstrated that increasing the number of imidazole units in poly(arylene ether ketone) polymers enhances their thermal stability.[13] By incorporating three precursors, it becomes possible to design pulsing sequences like ABCB (TMA + IPA + DAB + IPA) that can potentially result in two imidazole units within the PBI structure (Scheme 4). In contrast, the ABC type MLD sequence generates just one imidazole unit.

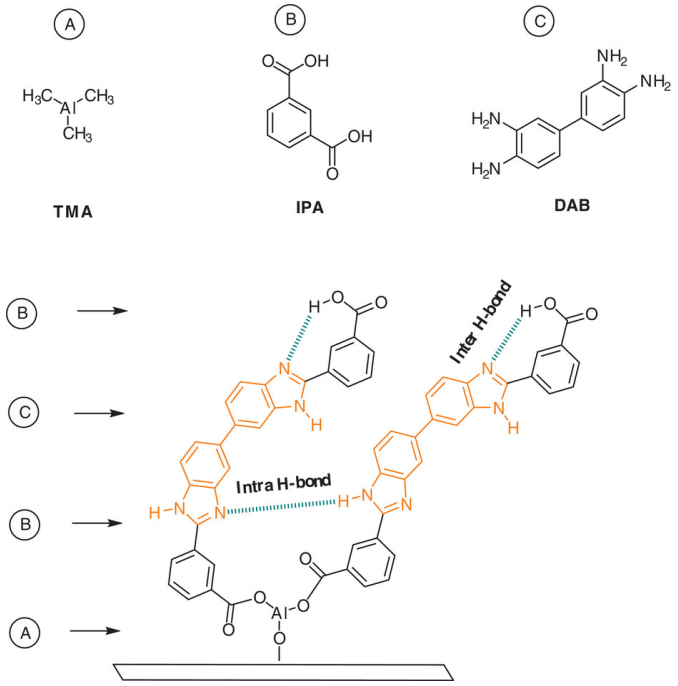

Scheme 4 Schematic representation of the proposed structure of a film deposited with the ABCB type TMA + IPA + DAB + IPA MLD process.

The ABCB cycle includes four steps (Equations 1-4). TMA is initially pulsed to create an -Al$(CH_3)_x$ terminated surface, which is highly reactive for the subsequent IPA precursor. The IPA molecules strongly bond to the surface, forming a carboxylic acid group that will react with DAB in the next step to create the imidazole ring structure. Without TMA, the IPA adsorption is probably so weak that the monomers

are purged away and no film growth occurs. The additional IPA pulse in the ABCB cycle aims to produce reactive carboxylic acid groups for the next TMA pulse, enhancing the surface reactivity and ensuring consistent film growth. While two imidazole units per cycle were expected in the ABCB pulsing sequence and one in the ABC sequence, the GPC was higher for the ABC sequence (7.0 Å) compared to ABCB (6.0 Å), and the aluminum content was higher than predicted, suggesting more complex reaction pathways than initially proposed.

A) $|\text{-OH} + \text{Al(CH}_3\text{)}_3\ (g) \longrightarrow |\text{-OAl(CH}_3\text{)}_2 + \text{CH}_4$ (1)

B) $|\text{-O-Al(CH}_3\text{)}_2 + 2\ \text{HOOC-}\mathbf{R}\text{-COOH}\ (g) \longrightarrow |\text{-O-Al-(OOC-}\mathbf{R}\text{-COOH)}_2 + 2\ \text{CH}_4\ (g)$ (2)

C) $|\text{-O-Al-(OOC-}\mathbf{R}\text{-COOH)}_2 + 2\ (\text{H}_2\text{N})_2\text{-}\mathbf{R}'\text{-(NH}_2\text{)}_2\ (g) \longrightarrow |\text{-O-Al-(OOC-}\mathbf{R}\text{-CNNH-}\mathbf{R}'\text{-(NH}_2\text{)}_2\text{)}_2 + 2\ \text{H}_2\text{O}\ (g)$ (3)

B) $|\text{-O-Al-(OOC-}\mathbf{R}\text{-CNNH-}\mathbf{R}'\text{-(NH}_2\text{)}_2\text{)}_2 + 2\ \text{HOOC-}\mathbf{R}\text{-COOH}\ (g) \longrightarrow |\text{-O-Al-(OOC-}\mathbf{R}\text{-CNNH-}\mathbf{R}'\text{-CNNH-}\mathbf{R}\text{-COOH)}_2 + 2\ \text{H}_2\text{O}$ (4)

Subsequently, we conducted a comprehensive analysis of the PBI-like films deposited using the ABCB type (TMA + IPA + DAB + IPA) MLD sequence. These analyses involved an examination of growth characteristics as well as a detailed evaluation of film properties, including their thermal and chemical stabilities.
It was observed that elevating the deposition temperature had the anticipated effect of decreasing the GPC, aligning with the behavior expected for MLD processes (Figure 16a). The thicknesses of the films displayed a linear dependence on the number of MLD cycles. On silicon substrates covered by the native oxide, a GPC value of 6.0 Å was determined (Figure 16b).

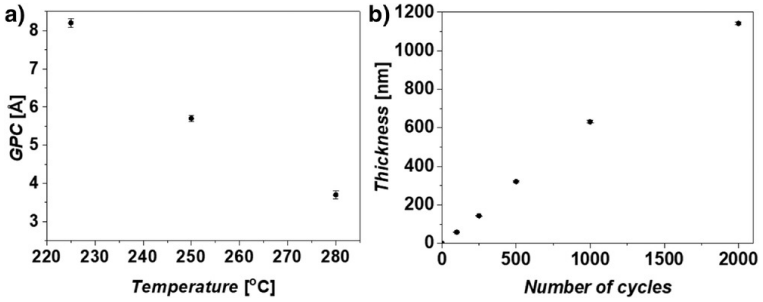

Figure 16 a) GPC as a function of the deposition temperature. b) Thicknesses of the PBI-like films deposited on silicon at 250 °C by the ABCB pulsing sequence as a function of the number of deposition cycles.

The saturation behavior of the growth was investigated by varying the pulse times of the precursors. It was observed that saturation was achieved with pulse lengths of 1.5 seconds for all the three precursors (Figure 17).

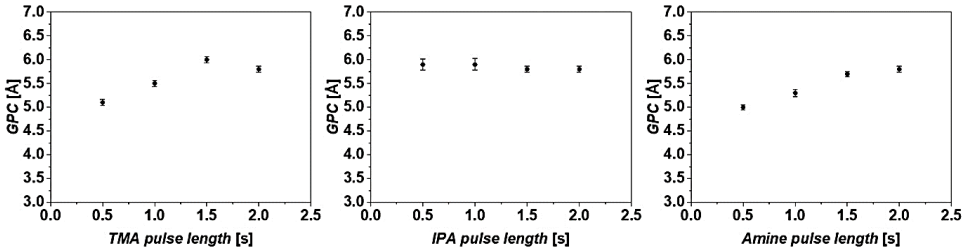

Figure 17 Saturation curves at 250 °C for each precursor in the ABCB (TMA + IPA + DAB + IPA) pulsing sequence.

4.2.1 PBI-like Film Structure and Morphology

We conducted a comparison of infrared (IR) spectra measured from films deposited with three different sequences (Figure 18). When pulsing only TMA and DAB at a temperature of 225°C, a film was deposited. However, it displayed a pronounced reactivity with the ambient air. This reactivity may likely be attributed to the presence of unreacted Al-CH_3 or amine groups within the films. This claim is supported by the observation of vibrational peaks corresponding to the primary amine -NH_2 groups in the IR spectra of the film deposited with the TMA + DAB sequence (Figure 18).

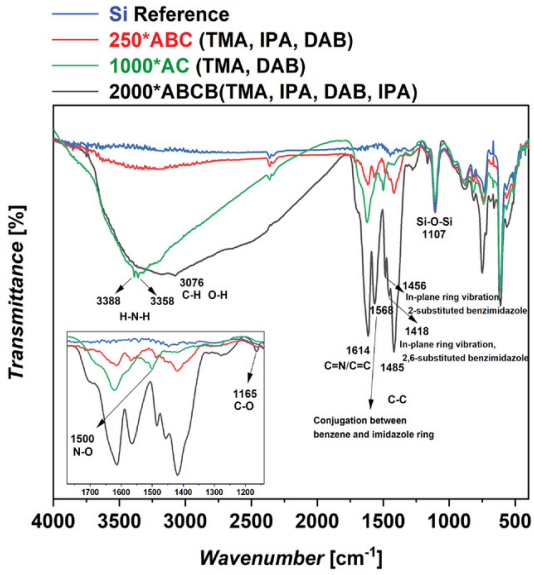

Figure 18 FTIR spectra of the ABC: TMA + IPA + DAB; AC: TMA + DAB; and ABCB: TMA + IPA + DAB + IPA type films deposited at 250, 220, and 250 °C, respectively.

The IR spectrum of the film deposited with the TMA + DAB sequence exhibited distinct characteristics, including the asymmetrical N-H stretch vibration at 3388 cm^{-1} and the symmetrical N-H stretch at 3358 cm^{-1}. Notably, the broad absorption above 3000 cm^{-1} indicated the presence of water absorbed from the ambient air, which functioned as a reactive agent within the resulting film. Additionally, absorptions detected around 1500 cm^{-1} could be attributed to the N-O stretching mode, indicative of the oxidation of the amine precursor upon exposure to the ambient air.

By incorporating IPA to the MLD sequence, stable films were successfully achieved at 250°C, exhibiting a GPC of 7.0 Å in the ABC sequence. This sequence facilitates the formation of imidazole units when isophthalic acid reacts with the DAB. In the ABCB sequence, a second imidazole unit is formed when the amine terminated surface from the DAB pulse reacts with the carboxylic acid groups during the subsequent IPA pulse.

FTIR spectrum revealed imidazole-type vibrations, providing evidence of the growth of a PBI-like film (Figure 18). The difference between the films deposited by the ABC and ABCB pulsing sequences is evidenced by a broad –NH vibrational peak in the ABC film, which is attributed to interchain hydrogen bonding. Both

sequences resulted in PBI-like films showing a low-intensity peak at 3076 cm^{-1}, associated with the stretching modes of aromatic C-H groups. A broad vibrational peak above 3000 cm^{-1} relates to the stretching vibrations of –OH functional groups from IPA and intrahydrogen bonding between the hydrogen in imidazole and the oxygen in carbonyl group from IPA. This peak can also result from hydrogen bonds between water molecules from ambient air and the imidazole units in the polymer. The region of 1650–1200 cm^{-1} is characteristic of benzimidazoles, displaying C=C/C=N stretching vibrations at 1614 cm^{-1} and ring modes indicative of benzene and imidazole ring conjugation at 1568 cm^{-1}. Strong absorptions due to in-plane ring modes are at 1456 and 1418 cm^{-1}, while an absorption band at 1165 cm^{-1} corresponds to C–O–H stretching modes of the unreacted hydroxyl groups of IPA. Surface morphology of the PBI-like film was examined using AFM (Figure 19). Notably, the surface of the 1.0 µm thick PBI film exhibited remarkably smooth appearance, with a low surface roughness value of Rq: 0.48 nm (measured within a 500 nm × 500 nm area, where Rq stands for root mean square roughness).

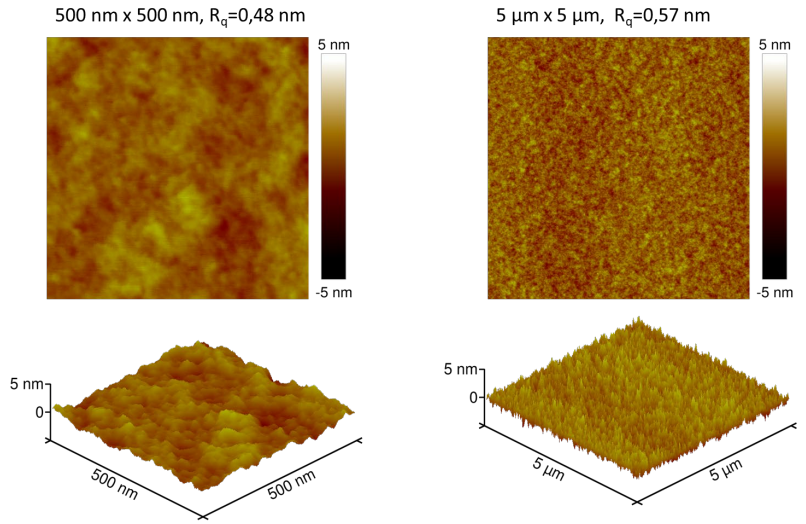

Figure 19 AFM images of 1 µm thick PBI-like film deposited at 250 °C with 2000 cycles on Si.

4.2.2 PBI-like Film Nanostructures

Nanostructures were made with the aim of exploring their potential in various high-performance device applications. The aim was to make durable, free-standing, and

tubular PBI-like films. This was achieved by coating electrospun polyvinylpyrrolidone (PVP) [127] fibers (Figure 20) and subsequently removing the template fibers by annealing or dissolution.

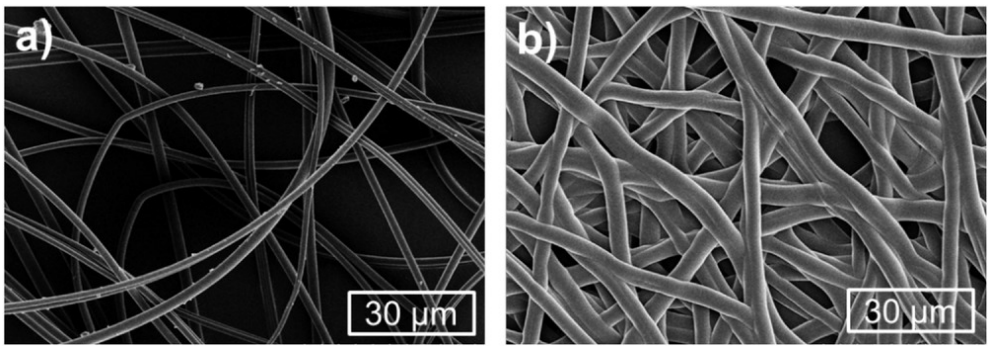

Figure 20 a) SEM images of electroblown PVP fibers and b) PBI-like coated PVP fibers obtained by MLD at 250 °C with 1000 cycles, resulting in a film thickness of ≈680 nm.

PVP fibers coated with the PBI-like films were subjected to annealing in air at 450 °C for durations of 4 and 10 hours. After 4 hours of annealing, the PVP had been completely combusted in air whereas the PBI-like film remained, as evidenced by SEM images that display distorted tubular structures (Figure 21).

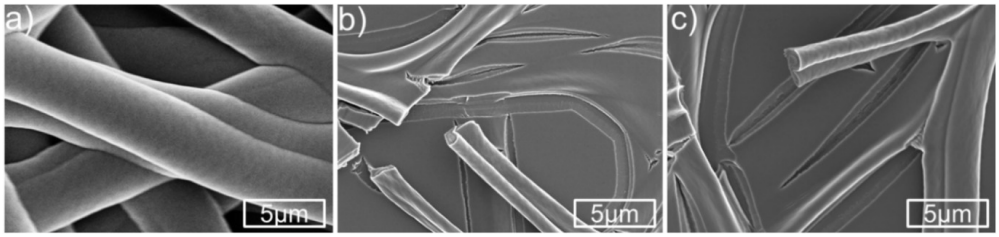

Figure 21 SEM images of PVP fibers coated with PBI-like a) as-deposited, and b) after annealing in air at 450 °C for 4 h and c) for 10 h.

The dissolution method for the removal of PVP fibers proved to be significantly gentler compared to the thermal combustion of PVP at 450 °C. The dissolution approach yielded tubular PBI structures (Figure 22) whereas the annealing resulted in distorted tubular structures.

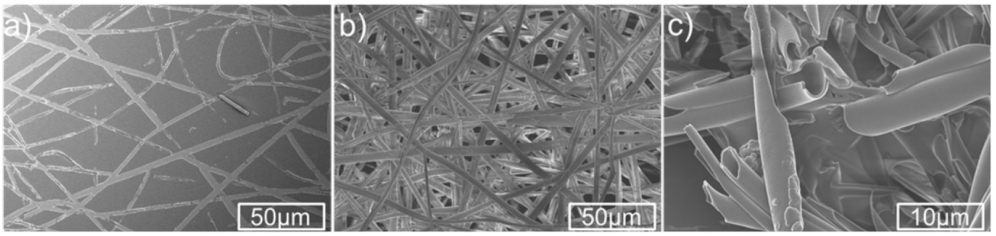

Figure 22 SEM images of PBI-like coated PVP fibers after treating with ethanol. a,b) tubular PBI-like structures, c) cracks of tubular PBI-like structures on the surface.

4.3 MLD of Polyimidazopyrrolone (Pyrrone) Thin Films

4.3.1 Pyrrone Film Growth

In Publication III the aim was to develop polymer materials with superior thermal stability and chemical resistance. These properties are crucial for advanced electronic and nanotechnology applications. Pyrrone thin films are particularly targeted for their potential use in high-temperature and chemically harsh environments where traditional polymer materials often fail. The high conformality and uniformity of the MLD process ensure that these films can be used in complex 3D structures, enhancing their utility in various cutting-edge technologies.

In this process, pyromellitic dianhydride (PMDA) and 3,3´-diaminobenzidine (DAB) were used as organic monomers, while ozone was used as a growth promoting precursor. In the initial experiments, pulsing of only PMDA and DAB at temperatures ranging from 220 to 300°C was also examined. Depositions conducted below 250°C resulted in GPC values of 2.3–2.7 Å. However, no saturative MLD conditions were achieved and nonuniform films were deposited.

As the temperature was increased, the quality of the films improved. Yet, the GPC decreased significantly, measuring only 0.12 Å on silicon substrates and around 2.0 Å on soda lime glass (Figure 23). This discrepancy might be attributed to different precursor bonding modes on the surfaces of soda lime glass and silicon. On silicon substrates, the GPC exhibited a minimum at 250°C, with a slight increase observed at higher temperatures. This rise in GPC is likely due to the increasing reactivity of the precursors.

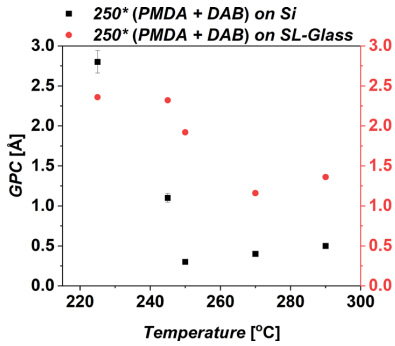

Figure 23 GPC as a function of deposition temperature on silicon and soda lime glass substrates when using a sequence 250x(PMDA+DAB) with 1.0 s pulses and purges of precursors.

We investigated the FTIR absorption spectrum of a film deposited on silicon at a temperature of 220°C, utilizing 250 MLD cycles. The purpose of this analysis was to identify specific functional groups and structure present within the film. The FTIR spectrum exhibited distinct vibrational peaks that could be attributed to the pyrrone structure, along with the formation of amide -N-C=O and -C=N bonds at 1722 cm^{-1} and 1623 cm^{-1}, respectively (Figure 24).

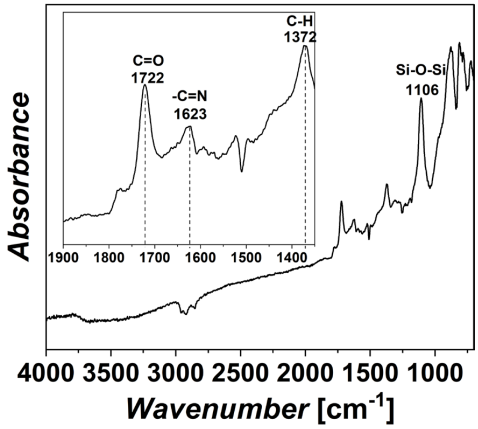

Figure 24 FTIR spectrum of a 27 nm polymer film deposited using 250 cycles of PMDA and DAB precursors on Si at 220 °C.

The impact of water, hydrogen peroxide, and oxygen as growth promoting precursors was investigated since no film uniformity and saturation of the growth were achieved without a promoting precursor. Among these options, ozone emerged as the most effective reactant in this process. The oxidant is expected to

facilitate condensation reactions between DAB and PMDA by creating new active sites in the molecules. DAB+PMDA+O_3 and DAB+O_3+PMDA precursor pulsing sequences were tested and they both yielded pyrrone films. Specifically, utilizing the DAB+PMDA+O_3 sequence led to a GPC of 1.5 Å, while the DAB+O_3+PMDA sequence resulted in a GPC of 1.2 Å, both being achieved at temperatures ranging from 250 to 300°C.

With the DAB+PMDA+O_3 pulsing sequence, the saturation behavior was observed with pulse lengths of 2.5 s, 2.0 s, and 0.2 s for DAB, PMDA, and O_3, respectively (Figure 25). Notably, the refractive index exhibited an increase with increasing DAB pulse lengths, ranging from 1.80 to 1.90. For the PMDA precursor, the refractive index remained consistently between 1.89 and 1.90 for all the tested pulse lengths. When varying the ozone pulse length, the refractive index displayed values close to 1.9 up to 2.0 s ozone pulse length, after which it started to decrease. Similar patterns were noted for the refractive indices in the saturation tests with the DAB+O_3+PMDA MLD sequence (Figure 26).

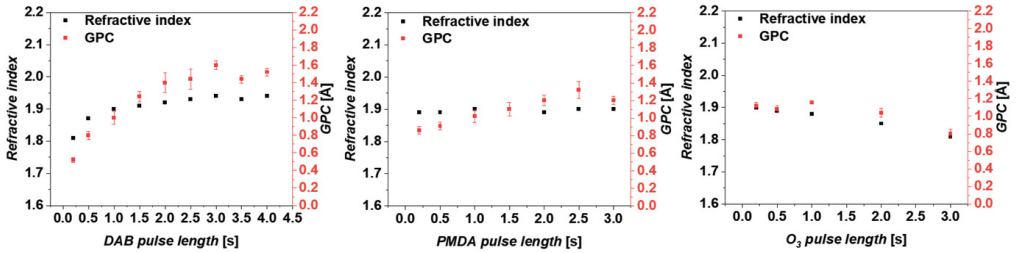

Figure 25 GPC and refractive indices in the DAB+PMDA+O_3 MLD sequence at 250 °C with 250 cycles.

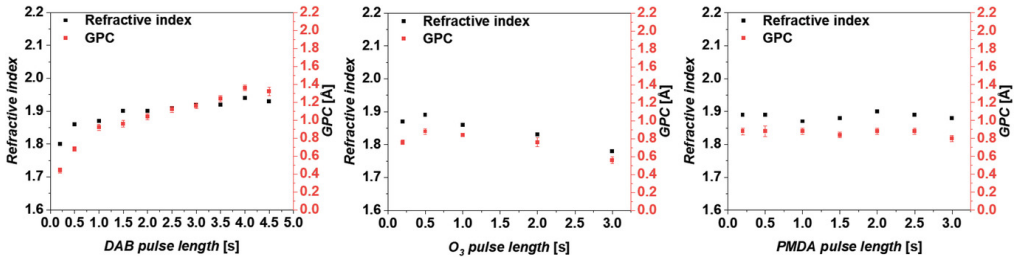

Figure 26 Saturation of GPC and refractive indices in the DAB+O_3+PMDA MLD sequence at 250 °C with 250 cycles.

A detailed FTIR analysis was conducted on films deposited by the DAB+O_3, DAB+PMDA+O_3, and DAB+O_3+PMDA sequences, revealing minor distinctions. The last two sequences exhibited identical spectra, with only the FTIR spectrum of DAB+PMDA+O_3 shown in Figure 27 for clarity. The FTIR spectra provided evidence of oxidation of the DAB monomer and subsequent polymer film formation. Regardless of the pulsing order in the MLD cycle, all polymer films displayed vibrational peaks at 1618 cm^{-1}, attributed to the stretching vibration of -C=N groups conjugated to the biphenyl structure within the DAB composition. This peak indicates formation of a polymerized indamine film which contains a high number of conjugated double bonds along the polymer chain. During the process the amine groups (-NH_2) in the DAB molecules were replaced by -C-NH groups, following the oxidation of DAB.[130] When PMDA was inserted into the indamine chain new cyclic amide and imine bonds formed into the polymer structure. On the other hand, as it is evident that PMDA and DAB react with each other at least partially, ozone can promote the growth by completing these reactions. This would also explain why the pulsing order of the three precursors has only a minor effect. Ozone facilitates the oxidative polymerization of DAB, resulting in a polymeric structure characterized by conjugated double bonds and amine-to-imine conversion.

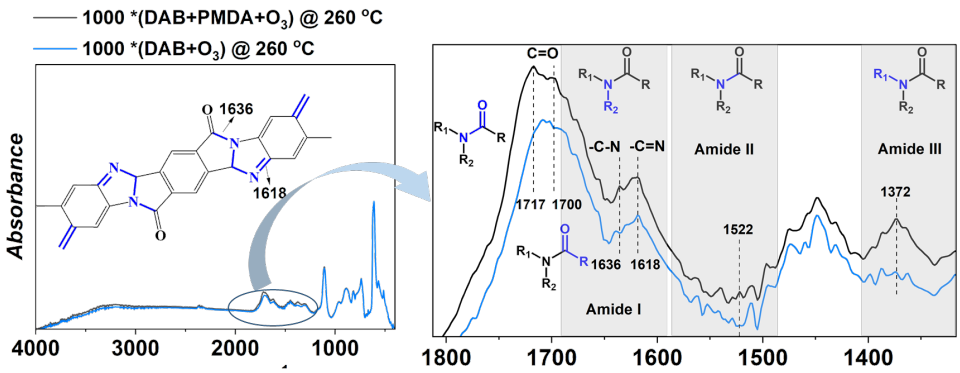

Figure 27 FTIR spectra of the films deposited with the DAB+O_3 and DAB+PMDA+O_3 MLD sequences at 260 °C with 1000 cycles of 2.5 and 0.2 s pulses for DAB+O_3, and 2.5, 2.0, and 0.2 s pulses for DAB+PMDA+O_3 sequences respectively. An enlarged view of the spectra in the left figure is shown on the right. The inset in the left figure shows the molecular structure of pyrrone thin film.

A vibrational peak at 1636 cm^{-1} was observed in the film deposited using the DAB+PMDA+O_3 and DAB+O_3+PMDA sequences. This peak is attributed to the

formation of the Amide I bond in the both MLD sequences. The formation of the amide bond is also evident from the appearance of a vibrational peak at 1717 cm^{-1}, corresponding to the stretching vibration of the amide carbonyl C=O bond. In the spectral range of 1650–1750 cm^{-1}, which encompasses vibrational frequencies of aromatic structures, a multi-peak region is evident. The addition of PMDA to the DAB+O_3 sequence broadens this region, indicating the incorporation of PMDA into the polymer films. A peak at 1522 cm^{-1} is attributed to the stretching vibrations of the Amide II in the film deposited using the DAB+PMDA+O_3 sequence, while the peak at 1372 cm^{-1} corresponds to the Amide III bond in the same polymer film. In summary, the FTIR analysis confirms the formation of pyrrone polymer through these MLD sequences.

4.4 Properties of the Films

4.4.1 Thermal Stability of PBI-like and Pyrrone

Thermal stability of both the PBI-like and pyrrone films, deposited on silicon substrates, was assessed through annealing experiments conducted in both nitrogen and air environments at various temperatures (300-450 °C) for two hours. During the annealing, both the PBI-like and pyrrone films decreased in thickness. Notably, when annealed in air, the reduction in thickness was more pronounced for both films as compared to annealing in nitrogen. At 400 °C, the PBI-like film thickness decreased approximately 10% and 28% in the first annealing in nitrogen and air respectively.

When annealed in nitrogen, the PBI-like films maintained excellent thermal stability up to 400°C, with no significant degradation. After re-annealing for two hours at 400°C, the film thickness remained unchanged, indicating that the initial thickness reduction during the first annealing was due to densification. Similarly, when annealed in air, the films also exhibited stability up to 400°C. This was the maximum temperature at which the PBI-like films showed thermal stability in both nitrogen and air, even after a second round of annealing, without further degradation.

When the PBI-like films were annealed in air at 450 °C they experienced gradual combustion in the first annealing and then second annealing for another two hours removed most of the film thickness. In contrast, 300°C was the highest temperature that the pyrrone films survived when annealed in air. Densification of the pyrrone film was observed at 300 °C as the film thickness decreased by 7%. At 450 °C, the pyrrone films experienced a rapid decrease in thickness within just one hour, indicative of rapid combustion in air.

4.4.2 Chemical Stability of PBI-like and Pyrrone Films

Both PBI and pyrrone polymers exhibit remarkable resistance to corrosive chemicals, including strong acids. To evaluate the stability of the PBI-like and pyrrone films, we subjected them to various tests involving different organic solvents as well as harsh acidic and basic solutions. Pyrrone polymer films demonstrated insolubility in commonly used organic solvents such as acetone, isopropanol, dimethylsulfoxide, dimethylformamide, dichloromethane, toluene, and acetonitrile. Detailed observations with SEM revealed that the pyrrone film remained intact after exposure to the organic solvents (Figure 28). Such an exceptional resistance against a wide range of organic solvents underscores the robustness and durability of pyrrone polymers in harsh chemical environments. Also the PBI-like films were stable in all the other solvents except dimethylsulfoxide that caused a minor decrease in the film thickness by a few nanometers.

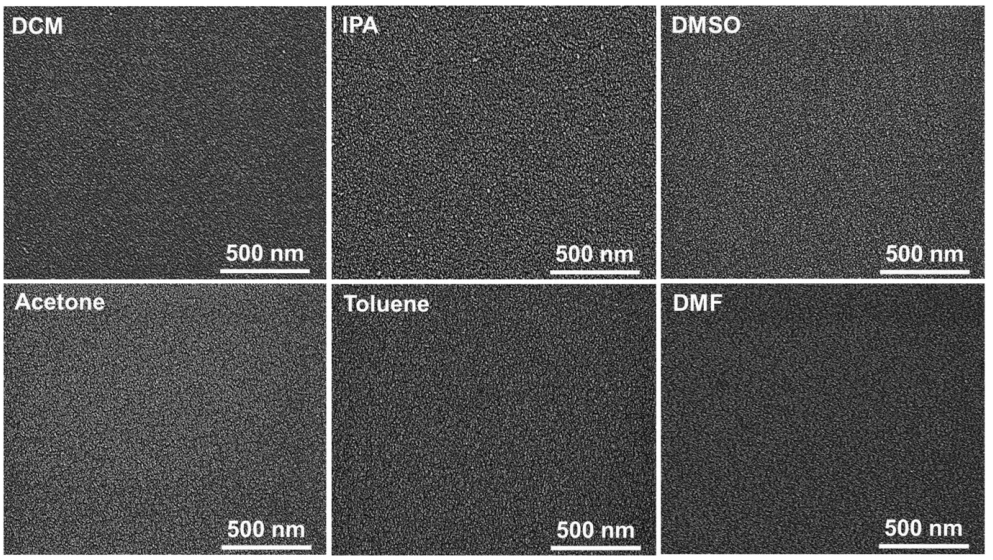

Figure 28 SEM images of the pyrrone films after 48 h immersion in organic solvents.

For assessing the stability of the films against corrosive substances, strong acid and base solutions were used, including H_2SO_4, HNO_3, HCl, and NaOH, at varying concentrations of 2%, 5%, and 10%. These solutions were allowed to equilibrate at room temperature for 24 hours prior to the test itself. Subsequently, the samples were rinsed with deionized water and dried in a furnace at 100°C for 48 hours to eliminate any residual water before analysis.

The results revealed that the pyrrone films remained insoluble in all the acid solutions, indicating their excellent resistance to strong acids. However, in the case of 10% HCl acid exposure, minor impurities were introduced into the film, as evident from SEM images (Figure 29). On the other hand, when subjected to NaOH solutions, the pyrrone films exhibited partial dissolution. Interestingly, within a few hours, the films began to detach from the substrate and floated on the surface of the solution. This flaking is attributed to the dissolution of the underlying native silicon oxide layer into NaOH. [131]

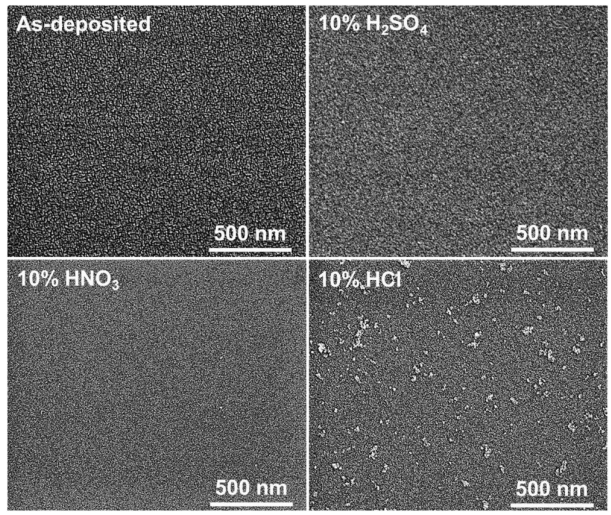

Figure 29 SEM images of the pyrrone films after exposure to strong acid solutions for 24 h.

Upon immersing 1 μm thick PBI-like films on silicon substrates into concentrated solutions of sulfuric acid, phosphoric acid, hydrochloric acid and formic acid, complete dissolution occurred within 24 hours. However, acetic acid exhibited no noticeable effect on the PBI-like film.

PBI-like films were subjected to also diluted acid solutions of H_2SO_4, H_3PO_4, HCOOH and HCl, at concentrations of 10%, 15% and 20% for 24 hours. While the film thicknesses decreased significantly from the initial 1 μm, the films did not dissolve completely into the diluted acid solutions. The thinnest remaining film was only 43 nm, measured after the 20% formic acid immersion. The highest remaining thickness was 135 nm, observed after subjecting the film to 15% sulfuric acid (Figure 30).

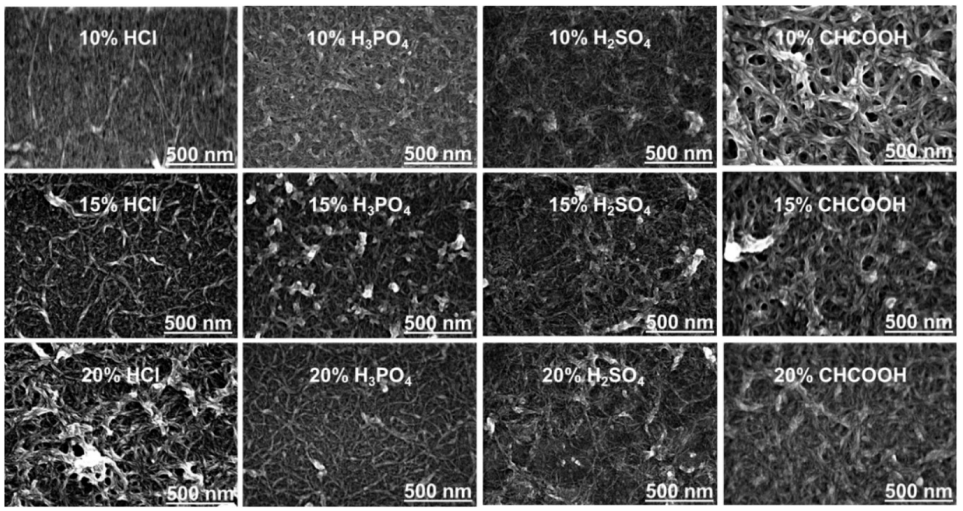

Figure 30 SEM images of 1 μm thick PBI-like thin films after 24 hours of immersion in diluted acid solutions.

4.4.3 Electrical and Optical Properties of MLD films

4.4.3.1 PEDOT Film

The as-deposited PEDOT films already exhibited excellent properties, achieving a conductivity of around 1200 S/cm (Figure 31). The water rinsing further enhanced quality of the films by effectively removing impurities, such as rhenium and chlorine left from the use of $ReCl_5$ as the oxidant. After water rinsing, the Re content was decreased from 1.6 at.% to 0.5 at.%, and Cl was no longer detectable. The decrease in impurities increased conductivity of the films to around 2000 S/cm.

Choosing proper post deposition treatment method is a key factor to further enhance conductivity of the films. For example, single crystals PEDOT nanowires with conductivities ranging from 7619 to 8797 Scm^{-1} were grown from EDOT monomers that were self-assembled and crystallized during VPP within nanoscale channels of a mold having $FeCl_3$ catalysts. Fe was removed by methanol washing but the Cl^- counter-anions remained in the PEDOT crystals so as to serve as a major dopant. Another example, PEDOT films deposited by oCVD method with $FeCl_3$ as oxidant and further treated with HBr water solution can reach electrical conductivities up to 6259 Scm^{-1}. But these post deposition treatments often require

complex, multi-step processes with hazardous chemicals. High conductivities were achieved here for the oMLD PEDOT films after the water rinsing. The water rinsing method is simple, safe, and environmentally friendly, offering a streamlined alternative without compromising the film quality.

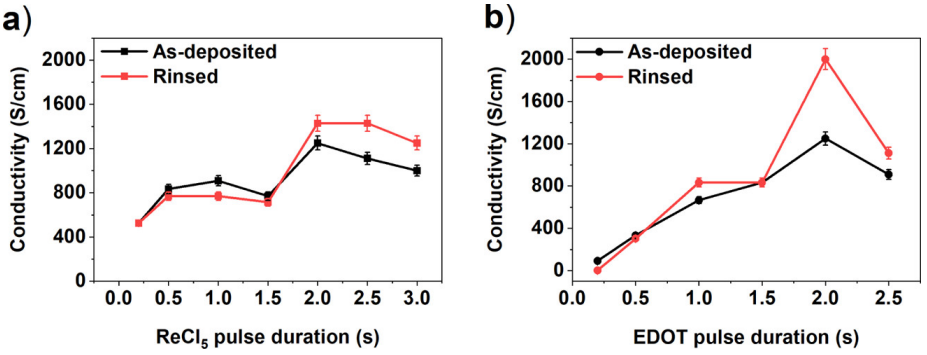

Figure 31 Conductivity of the as-deposited and water-rinsed samples. Effect of (a) $ReCl_5$ pulse duration and (b) EDOT pulse duration.

The films subjected to rinsing also exhibited increased transmittance in comparison to the as-deposited films. Among the rinsed films, the highest transmittance value reached 80%, whereas the corresponding value for the as-deposited film was 75%. On the as-deposited films the particles decrease transmittance by scattering the light.

4.4.3.2 PBI-like and Pyrrone Films

PBI-like and pyrrone films, unlike PEDOT, are insulators. To assess their electrical properties capacitor structures were constructed from PBI-like and pyrrone films deposited onto indium tin oxide substrates. Top electrodes composed of aluminium dots were evaporated onto the polymer layer. Dielectric constants were determined by measuring the capacitance. Uniformity across various locations on the substrate was verified by a negligible variance observed in the capacitances.

For a 76 nm thick PBI-like film, the evaluated dielectric constant was 4.9. The leakage current of the same film remained below 1 μA cm^{-2} under a 10 V bias. In most of the tested devices, dielectric breakdown occurred around 24 V, indicative of reasonably good insulating characteristics of the PBI-like polymer film. In the

literature a dielectric constant of 4.4 was measured for 38 μm thick PBI film deposited by casting a polymeric solution on to the substrate.[132]

Dielectric constant of a 91 nm thick pyrrone films at room temperature was 5.2. The leakage current of the MLD pyrrone film was measured in both light and dark conditions to assess the photoelectric properties of the material. By comparing the leakage currents in these two conditions, sensitivity of the film to light, its potential use in optoelectronic devices, and how it behaves under different environmental conditions can be determined. This analysis helps in understanding charge transport mechanisms and the effect of light on the electrical properties of the pyrrone films. In the literature,[133] dielectric constant of 3.2–3.3 was measured for 10-15 μm thick pyrrone films deposited by casting a polymeric solution on to the substrate. The photocurrent-to-dark current ratio of casted pyrrone (PMDA-DAB) films at room temperature ranged from 40 to 60 when exposed to polychromatic light with an intensity of 10-20 mW/cm². This indicated that the photocurrent is substantially higher than the dark current, reflecting the photoconducting nature of the material. [134]

Pyrrone films in publication III were tested for their photoconductivity properties. Upon application of bias voltages, the devices exhibited an immediate response to light from a 200 W halogen lamp, without local heating, as it is seen in the light curve in Figure 32. Under 5 V voltage, the current remained stable throughout the measurement, exhibiting consistent response. The light curve demonstrates that the pyrrone films have stable electrical properties under illumination, making them suitable for applications where light exposure is a factor, such as photodetectors and other optoelectronic devices. However, when voltages of 7 V and higher were applied, the devices demonstrated signs of aging. The dark curve, representing the leakage current of the ITO/pyrrone/Al capacitor, remained low. As both the dark and light currents were minimal (Figure 32), the illumination did not influence the measured capacitance.

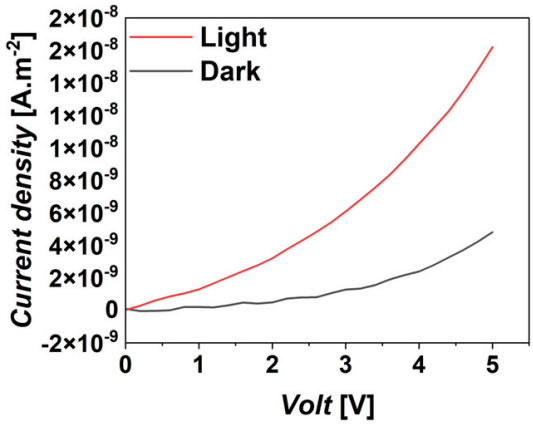

Figure 32 Current densities of the ITO/pyrrone/Al capacitor in light and dark.

5 Conclusions

Through the exploration of novel organic materials for MLD, this thesis aims to broaden the spectrum of materials applicable for the fabrication of polymeric thin films. In essence, the primary objective of these investigations was to design MLD processes that could overcome the inherent temperature constraints often associated with films made by MLD. By leveraging carefully chosen organic monomers and deposition temperatures, we deposited films that effectively achieved the desired thermal stability and chemical resistance characteristics. These discoveries offer promises across a range of applications where qualities like robustness against high temperatures and chemical stability are crucial, including microelectronics, energy related applications and protective coatings.

The research began with an exploration of $ReCl_5$ and its potential for oxidizing EDOT to deposit PEDOT thin films, motivated by its structural and chemical similarities to the earlier used $MoCl_5$. Subsequent investigations aimed to overcome temperature-related challenges inherent in MLD processes. By incorporating organic monomers, linker and growth promoting reactants, the goal was to design processes to deposit polymer thin films capable of withstanding elevated temperatures. In one study, the combination of DAB and IPA as monomers, along with TMA as a linker, facilitated the growth of PBI-like MLD films. Another study utilized DAB and PMDA as organic monomers, with ozone as a growth promoting precursor, resulting in the deposition of pyrrone thin films. Both film materials exhibited exceptional thermal stability and chemical resistance against harsh environments, including acidic solutions and organic solvents.

These newly developed materials hold significant promise for a range of applications spanning electronics, sensors, fuel cells, and barrier coatings. The outcomes of this research significantly contribute to the progression of MLD as a viable technique for producing top-quality polymer thin films. The field of MLD remains largely unexplored, offering numerous opportunities for exploration and

creativity in terms of material advancement. Future research could focus on further enhancing the electrical and thermal performance of these films to meet the evolving needs of advanced electronic devices and high-performance energy systems. Exploring the integration of these robust films with emerging technologies such as flexible electronics, wearable devices, and next-generation batteries could open new avenues for innovation.

6 References

[1] A. Kubono, N. Okui, Polymer thin films prepared by vapor deposition, Progress in Polymer Science 19 (1994) 389-438. https://doi.org/10.1016/0079-6700(94)90001-9

[2] S.H. Whang, Nanostructured metals and alloys : processing, microstructure, mechanical properties and applications, Woodhead Publishing, Elsevier Ltd. (2011) 1–803. https://doi.org/10.1533/9780857091123

[3] V. Ruiz, Á. Colina, A. Heras, J. López-Palacios, Electropolymerization under potentiodynamic and potentiostatic conditions Spectroelectrochemical study on electrosynthesis of poly[4,4′-bis(2-methylbutylthio)-2,2′-bithiophene], Electrochim Acta 50 (2004) 59–67. https://doi.org/10.1016/j.electacta.2004.07.013

[4] S.Y. Moon, E. Jeon, J.S. Bae, M. Byeon, J.W. Park, Polyurea networks via organic sol-gel crosslinking polymerization of tetrafunctional amines and diisocyanates and their selective adsorption and filtration of carbon dioxide, Polym Chem 5 (2014) 1124–1131. https://doi.org/10.1039/c3py01593a

[5] T. Yoshimura, S. Tatsuura, W. Sotoyama, Polymer films formed with monolayer growth steps by molecular layer deposition, Appl Phys Lett 59 (1991) 482–484. https://doi.org/10.1063/1.105415

[6] G. Ozaydin-Ince, A.M. Coclite, K.K. Gleason, CVD of polymeric thin films: applications in sensors, biotechnology, microelectronics/organic electronics, microfluidics, MEMS, composites and membranes, Reports on Progress in Physics 75 (2012) 016501. https://doi.org/10.1088/0034-4885/75/1/016501

[7] H. Vogel, C.S. Marvel, Polybenzimidazoles, new thermally stable polymers, J Polym Sci A Polym Chem 34 (1996) 1125–1153. https://doi.org/10.1002/pola.1996.826

[8] A. Banihashemi, F. Atabaki, Synthesis and characterization of new thermally stable polybenzimidazoles and poly(amide-benzimidazole)s, Eur Polym J 38 (2002) 2119–2124. https://doi.org/10.1016/S0014-3057(02)00081-2

[9] G.P. Karayannidis, I. Sideridou-Karayannidou, Synthesis and properties of pyrrones containing p-benzoquinone units, Journal of Macromolecular Science: Part A - Chemistry 23 (1986) 157–167. https://doi.org/10.1080/00222338608063384

[10] I. Sideridou-Karayannidou, G. Karayannidis, Synthesis of pyrrones based on the reduction and cyclization of their o-nitrosubstituted polyimides precursors, Die Angewandte Makromolekulare Chemie 180 (1990) 121–129. https://doi.org/10.1002/apmc.1990.051800109

[11] Morgan, P. E. D., Scott, H. Simultaneous polymerization and molding of pyrrone polymers, NASA Contractor Reports 16 (1971) 2029–2050. https://doi.org/10.1002/app.1972.070160815

[12] J. Liao, Y. Chu, J. Wang, M. Zhou, Y. Cao, Dielectric and gas transport properties of the films of thermally stable poly(arylene ether ketone)s containing content-tunable benzimidazole moiety, J Appl Polym Sci 132 (2015). https://doi.org/10.1002/app.41289

[13] F. Hu, W. Zhang, Y. Xue, K. Lin, B. Lu, J. Xu, G. Zhao, Tuning optoelectronic performances for 3-methylselenophene-EDOT hybrid polymer, Mater Chem Phys 244 (2020) 122699. https://doi.org/10.1016/j.matchemphys.2020.122699

[14] P. Yadav, S. Naqvi, A. Patra, Poly(3,4-ethylenedioxyselenophene): effect of solvent and electrolyte on electrodeposition, optoelectronic and electrochromic properties, RSC Adv 10 (2020) 12395–12406. https://doi.org/10.1039/d0ra01436b

[15] D.C. Borrelli, S. Lee, K.K. Gleason, Optoelectronic properties of polythiophene thin films and organic TFTs fabricated by oxidative chemical vapor deposition, J Mater Chem C Mater 2 (2014) 7223–7231. https://doi.org/10.1039/c4tc00881b

[16] M. Heydari Gharahcheshmeh, M.T. Robinson, E.F. Gleason, K.K. Gleason, Optimizing the optoelectronic properties of face-on oriented poly(3,4-ethylenedioxythiophene) via water-assisted oxidative chemical vapor deposition, Adv Funct Mater 31 (2021) 1–12. https://doi.org/10.1002/adfm.202008712

[17] Y. Jia, L. Shen, J. Liu, W. Zhou, Y. Du, J. Xu, C. Liu, G. Zhang, Z. Zhang, F. Jiang, An efficient PEDOT-coated textile for wearable thermoelectric generators and strain sensors, J Mater Chem C Mater 7 (2019) 3496–3502. https://doi.org/10.1039/c8tc05906c

[18] L. Shen, P. Liu, C. Liu, Q. Jiang, J. Xu, X. Duan, Y. Du, F. Jiang, Advances in efficient polymerization of solid-state trithiophenes for organic thermoelectric thin-film,

ACS Appl Polym Mater 2 (2020) 376–384. https://doi.org/10.1021/acsapm.9b00842

[19] Z.U. Khan, O. Bubnova, M.J. Jafari, R. Brooke, X. Liu, R. Gabrielsson, T. Ederth, D.R. Evans, J.W. Andreasen, M. Fahlman, X. Crispin, Acido-basic control of the thermoelectric properties of poly(3,4-ethylenedioxythiophene)tosylate (PEDOT-Tos) thin films, J Mater Chem C Mater 3 (2015) 10616–10623. https://doi.org/10.1039/c5tc01952d

[20] A. Kalathil, A. Raghavan, B. Kandasubramanian, Polymer fuel cell based on polybenzimidazole membrane: a review, Polymer-Plastics Technology and Materials 58 (2019) 465–497. https://doi.org/10.1080/03602559.2018.1482919

[21] F. Group, Foundations of high performance polymers: properties, performance and applications (1st ed.), Apple Academic Press (2013) 14–16. https://doi.org/10.1201/b15485-2

[22] J. Ouyang, Recent advances of intrinsically conductive polymers, Acta Physico-Chimica Sinica 34 (2018) 1211–1220. https://doi.org/10.3866/PKU.WHXB201804095

[23] M. Sawatzki-Park, S.J. Wang, H. Kleemann, K. Leo, Highly ordered small molecule organic semiconductor thin-films enabling complex, high-performance multi-junction devices, Chem Rev 123 (2023) 8232–8250. https://doi.org/10.1021/acs.chemrev.2c00844

[24] K. Ariga, Organized organic ultrathin films : fundamentals and applications, Wiley-VCH (2013) 1–203. https://doi.org/10.1002/9783527654666.

[25] D.B. Mitzi, Thin-film deposition of organic-inorganic hybrid materials, Chemistry of Materials 13 (2001) 3283–3298. https://doi.org/10.1021/cm0101677

[26] K. Ashurbekova, K. Ashurbekova, G. Botta, O. Yurkevich, M. Knez, M. Knez, Vapor phase processing: a novel approach for fabricating functional hybrid materials, Nanotechnology 31 (2020) 342001–342033. https://doi.org/10.1088/1361-6528/ab8edb

[27] S.H. Mir, L.A. Nagahara, T. Thundat, P. Mokarian-Tabari, H. Furukawa, A. Khosla, Review—organic-inorganic hybrid functional materials: an integrated platform for applied technologies, J Electrochem Soc 165 (2018) B3137–B3156. https://doi.org/10.1149/2.0191808jes

[28] Z.-Q. Shi, N.-N. Ji, L.-L. Lan, T. Zhang, H.-L. Hu, G. Li, Recent progress of metal–organic coordination polymers built by aromatic fused-thiophen functionalized

ligands, Coord Chem Rev 493 (2023) 215300. https://doi.org/10.1016/j.ccr.2023.215300

[29] L. Nicole, L. Rozes, C. Sanchez, Integrative approaches to hybrid multifunctional materials: from multidisciplinary research to applied technologies., Adv Mater 22 (2010) 3208–3214. https://doi.org/10.1002/adma.201000231

[30] C. Sanchez, G.J.D.A.A. Soler-Illia, F. Ribot, T. Lalot, C.R. Mayer, V. Cabuil, Designed hybrid organic-inorganic nanocomposites from functional nanobuilding blocks, Chemistry of Materials 13 (2001) 3061–3083. https://doi.org/10.1021/cm011061e

[31] G.J.D.A.A. Soler-Illia, C. Sanchez, B. Lebeau, J. Patarin, Chemical strategies to design textured materials: from microporous and mesoporous oxides to nanonetworks and hierarchical structures, Chem Rev 102 (2002) 4093–4138. https://doi.org/10.1021/cr0200062

[32] G.A. Ozin, Panoscopic materials: synthesis over "all" length scales, Chemical Communications (2000) 419–432. https://doi.org/10.1039/a905090f

[33] D.J. Tranchemontagne, J.L. Tranchemontagne, M. O'keeffe, O.M. Yaghi, Secondary building units, nets and bonding in the chemistry of metal–organic frameworks, Chem Soc Rev 38 (2009) 1257–1283. https://doi.org/10.1039/b817735j

[34] B. Devincre, T. Hoc, L. Kubin, Dislocation mean free paths and strain hardening of crystals, Science (1979) 320 (2008) 1745–1748. https://doi.org/10.1126/science.1156101

[35] J.C. Vartuli, C.T. Kresge, W.J. Roth, S.B. Mccullen, J.S. Beck, K.D. Schmitt, M.E. Leonowicz, J.D. Lutner, E.W. Sheppard, Designed synthesis of mesoporous molecular sieve systems using surfactant-directing agents, Advanced Catalysts and Nanostructured Materials, Elsevier (1996) 1–19. https://doi.org/10.1016/b978-012508460-4/50002-4

[36] S. Kitagawa, M. Kondo, Functional micropore chemistry of crystalline metal complex-assembled compounds, Bulletin of the Chemical Society of Japan 71 (1998) 1739–1753. https://doi.org/10.1246/bcsj.71.1739

[37] L.E. Kreno, K. Leong, O.K. Farha, M. Allendorf, R.P. Van Duyne, J.T. Hupp, Metal-organic framework materials as chemical sensors, Chem Rev 112 (2012) 1105–1125. https://doi.org/10.1021/cr200324t

[38] M.D. Allendorf, A. Schwartzberg, V. Stavila, A.A. Talin, A roadmap to implementing metal-organic frameworks in electronic devices: challenges and critical directions,

Chemistry - A European Journal 17 (2011) 11372–11388. https://doi.org/10.1002/chem.201101595

[39] Y. Chen, S. Ma, Microporous lanthanide metal-organic frameworks, Reviews in Inorganic Chemistry 32 (2012) 81–100. https://doi.org/10.1515/revic-2012-0003

[40] J.L.C. Rowsell, O.M. Yaghi, Metal-organic frameworks: a new class of porous materials, Microporous and Mesoporous Materials 73 (2004) 3–14. https://doi.org/10.1016/j.micromeso.2004.03.034

[41] J.L.C. Rowsell, O.M. Yaghi, Effects of functionalization, catenation, and variation of the metal oxide and organic linking units on the low-pressure hydrogen adsorption properties of metal-organic frameworks, J Am Chem Soc 128 (2006) 1304–1315. https://doi.org/10.1021/ja056639q

[42] M. C. Petty, Langmuir-Blodgett films, Endeavour 7 (2004) 65–69. https://doi.org/10.1016/S0160-9327(83)80004-0

[43] A. Ulman, An introduction to ultrathin organic films : from Langmuir-Blodgett to self-assembly, Academic Press (1991) 1–443. https://doi.org/10.1016/C2009-0-22306-3

[44] S. Kumar, D.K. Aswal Editors, Recent advances in thin films, organic thin films: Langmuir monolayers and multilayers, Springer, Singapore (2020) 345—368. http://www.springer.com/series/16122

[45] M.N. Gueye, A. Carella, J. Faure-Vincent, R. Demadrille, J.P. Simonato, Progress in understanding structure and transport properties of PEDOT-based materials: a critical review, Prog Mater Sci 108 (2020). https://doi.org/10.1016/j.pmatsci.2019.100616

[46] M. Fabretto, M. Müller, C. Hall, P. Murphy, R.D. Short, H.J. Griesser, In-situ QCM-D analysis reveals four distinct stages during vapour phase polymerisation of PEDOT thin films, Polymer (Guildf) 51 (2010) 1737–1743. https://doi.org/10.1016/j.polymer.2010.02.019

[47] J.P. Lock, S.G. Im, K.K. Gleason, Oxidative chemical vapor deposition of electrically conducting poly(3,4-ethylenedioxythiophene) films, Macromolecules 39 (2006) 5326–5329. https://doi.org/10.1021/ma060113o

[48] Y. Takahashi, M. Iijima, K. Inagawa, A. Itoh, Synthesis of aromatic polyimide film by vacuum deposition polymerization, Journal of Vacuum Science & Technology A: Vacuum, Surfaces, and Films 5 (1987) 2253–2256. https://doi.org/10.1116/1.574429

[49] D. Bhattacharyya, R.M. Howden, D.C. Borrelli, K.K. Gleason, Vapor phase oxidative synthesis of conjugated polymers and applications, J Polym Sci B Polym Phys 50 (2012) 1329–1351. https://doi.org/10.1002/polb.23138

[50] H.L. Shao, S. Umemoto, T. Kikutani, N. Okui, Layer-by-layer polycondensation of nylon 66 by alternating vapour deposition polymerization, Polymer (Guildf) 38 (1997) 459–462. https://doi.org/10.1016/S0032-3861(96)00504-6

[51] M.L. Petrus, R.K.M. Bouwer, U. Lafont, D.H.K. Murthy, R.J.P. Kist, M.L. Böhm, Y. Olivier, T.J. Savenije, L.D.A. Siebbeles, N.C. Greenham, T.J. Dingemans, Conjugated poly(azomethine)s via simple one-step polycondensation chemistry: synthesis, thermal and optoelectronic properties, Polym Chem 4 (2013) 4182–4191. https://doi.org/10.1039/c3py00433c

[52] J.-S. Kim, H. Oh, G.N. Parsons, Growth behavior and substrate selective deposition of polypyrrole, polythiophene, and polyaniline by oxidative chemical vapor deposition and molecular layer deposition, Journal of Vacuum Science & Technology A 40 (2022) 063401. https://doi.org/10.1116/6.0002036

[53] B. Winther-Jensen, J. Chen, K. West, G. Wallace, Vapor phase polymerization of pyrrole and thiophene using iron(III) sulfonates as oxidizing agents, Macromolecules 37 (2004) 5930–5935. https://doi.org/10.1021/ma049365k

[54] M.E. Alf, A. Asatekin, M.C. Barr, S.H. Baxamusa, H. Chelawat, G. Ozaydin-Ince, C.D. Petruczok, R. Sreenivasan, W.E. Tenhaeff, N.J. Trujillo, S. Vaddiraju, J. Xu, K.K. Gleason, Chemical vapor deposition of conformal, functional, and responsive polymer films, Advanced Materials 22 (2010) 1993–2027. https://doi.org/10.1002/adma.200902765

[55] H. Yasuda, H. Toshihiro, Critical evaluation of conditions of plasma polymerization, Journal of Polymer Science Part A 16 (1978) 743-759. https://doi.org/10.1002/pol.1978.170160403

[56] T.B. Casserly, K.K. Gleason, Effect of substrate temperature on the plasma polymerization of poly(methyl methacrylate), Chemical Vapor Deposition 12 (2006) 59–66. https://doi.org/10.1002/cvde.200506409

[57] K.K.S. Lau, J.A. Caulfield, K.K. Gleason, Structure and morphology of fluorocarbon films grown by hot filament chemical vapor desposition, Chemistry of Materials 12 (2000) 3032–3037. https://doi.org/10.1021/cm000499w

[58] X. Wang, X. Zhang, L. Sun, D. Lee, S. Lee, M. Wang, J. Zhao, Y. Shao-Horn, M. Dincă, T. Palacios, K.K. Gleason, High electrical conductivity and carrier mobility in oCVD

PEDOT thin films by engineered crystallization and acid treatment, Sci Adv 4 (2018) 1–10. https://doi.org/10.1126/sciadv.aat5780

[59] S.H. Baxamusa, L. Montero, J.M. Dubach, H.A. Clark, S. Borros, K.K. Gleason, Protection of sensors for biological applications by photoinitiated chemical vapor deposition of hydrogel thin films, Biomacromolecules 9 (2008) 2857–2862. https://doi.org/10.1021/bm800632d

[60] S.H. Baxamusa, S.G. Im, K.K. Gleason, Initiated and oxidative chemical vapor deposition: a scalable method for conformal and functional polymer films on real substrates, Physical Chemistry Chemical Physics 11 (2009) 5227–5240. https://doi.org/10.1039/b900455f

[61] J. Multia, M. Karppinen, Atomic/Molecular layer deposition for designer's functional metal–organic materials, Adv Mater Interfaces 2200210 (2022) 2200210. https://doi.org/10.1002/admi.202200210

[62] M. Madadi, J. Heiska, J. Multia, M. Karppinen, Atomic and molecular layer deposition of alkali metal based thin films, ACS Appl Mater Interfaces 13 (2021) 56793–56811. https://doi.org/10.1021/acsami.1c17519

[63] L. Svärd, M. Putkonen, E. Kenttä, T. Sajavaara, F. Krahl, M. Karppinen, K. Van De Kerckhove, C. Detavernier, P. Simell, Low-temperature molecular layer deposition using monofunctional aromatic precursors and ozone-based ring-opening reactions, Langmuir 33 (2017) 9657–9665. https://doi.org/10.1021/acs.langmuir.7b02456

[64] X. Meng, An overview of molecular layer deposition for organic and organic-inorganic hybrid materials: mechanisms, growth characteristics, and promising applications, J Mater Chem A Mater 5 (2017) 18326–18378. https://doi.org/10.1039/c7ta04449f

[65] P. Sundberg, M. Karppinen, Organic and inorganic-organic thin film structures by molecular layer deposition: a review, Beilstein Journal of Nanotechnology 5 (2014) 1104–1136. https://doi.org/10.3762/bjnano.5.123

[66] M. Putkonen, J. Harjuoja, T. Sajavaara, L. Niinistö, Atomic layer deposition of polyimide thin films, J Mater Chem 17 (2007) 664–669. https://doi.org/10.1039/b612823h

[67] D.S. Bergsman, R.G. Closser, S.F. Bent, Mechanistic studies of chain termination and monomer absorption in molecular layer deposition, Chemistry of Materials 30 (2018) 5087–5097. https://doi.org/10.1021/acs.chemmater.8b01468.

[68] R.A. Nye, A.P. Kelliher, J.T. Gaskins, P.E. Hopkins, G.N. Parsons, Understanding molecular layer deposition growth mechanisms in polyurea via picosecond acoustics analysis, Chemistry of Materials 32 (2020) 1553–1563. https://doi.org/10.1021/acs.chemmater.9b04702

[69] H. Jain, P. Poodt, About the importance of purge time in molecular layer deposition of alucone films, Dalton Transactions 50 (2021) 5807–5818. https://doi.org/10.1039/d1dt00623a

[70] R.A. Nye, S. Wang, S. Uhlenbrock, J.A. Smythe, G.N. Parsons, In situ analysis of growth rate evolution during molecular layer deposition of ultra-thin polyurea films using aliphatic and aromatic precursors, Dalton Transactions 51 (2022) 1838–1849. https://doi.org/10.1039/d1dt03689k

[71] A.A. Dameron, D. Seghete, B.B. Burton, S.D. Davidson, A.S. Cavanagh, J.A. Bertrand, S.M. George, Molecular layer deposition of alucone polymer films using trimethylaluminum and ethylene glycol, Chemistry of Materials 20 (2008) 3315–3326. https://doi.org/10.1021/cm7032977

[72] S.M. George, A.A. Dameron, B. Yoon, Surface chemistry for molecular layer deposition of organic and hybrid organic-inorganic polymers, Acc Chem Res 42 (2009) 498–508. https://doi.org/10.1021/ar800105q

[73] Q.K. Wyatt, K.G. Brathwaite, M. Ardiansyah, N.C. Paranamana, K.R. Brorsen, M.J. Young, Mechanistic insights into oxidative molecular layer deposition of conjugated polymers, Chemistry of Materials 35 (2023) 154–162. https://doi.org/10.1021/acs.chemmater.2c02923

[74] A.A. Volk, J.-S. Kim, J. Jamir, E.C. Dickey, G.N. Parsons, Oxidative molecular layer deposition of PEDOT using volatile antimony(V) chloride oxidant, Journal of Vacuum Science & Technology A 39 (2021) 032413. https://doi.org/10.1116/6.0000791

[75] C. Prasittichai, H. Zhou, S.F. Bent, Area selective molecular layer deposition of polyurea films, ACS Appl Mater Interfaces 5 (2013) 13391–13396. https://doi.org/10.1021/am4043195

[76] J.S. Lee, Y.-J. Lee, E.L. Tae, Y.S. Park, K.B. Yoon, Synthesis of zeolite as ordered multicrystal arrays, Science 301 (2003) 818 - 821. https://doi.org/10.1126/science.1086441

[77] P.W. Loscutoff, H.B.R. Lee, S.F. Bent, Deposition of ultrathin polythiourea films by molecular layer deposition, Chemistry of Materials 22 (2010) 5563–5569. https://doi.org/10.1021/cm1016239

[78] T. V. Ivanova, P.S. Maydannik, D.C. Cameron, Molecular layer deposition of polyethylene terephthalate thin films, Journal of Vacuum Science & Technology A: Vacuum, Surfaces, and Films 30 (2012) 01A121. https://doi.org/10.1116/1.3662846

[79] T. Yoshimura, R. Ebihara, A. Oshima, Polymer wires with quantum dots grown by molecular layer deposition of three source molecules for sensitized photovoltaics, Journal of Vacuum Science & Technology A: Vacuum, Surfaces, and Films 29 (2011). https://doi.org/10.1116/1.3620644

[80] N.M. Adamczyk, A.A. Dameron, S.M. George, Molecular layer deposition of poly(p-phenylene terephthalamide) films using terephthaloyl chloride and p-phenylenediamine, Langmuir 24 (2008) 2081–2089. https://doi.org/10.1021/la7025279

[81] S.E. Atanasov, M.D. Losego, B. Gong, E. Sachet, J.P. Maria, P.S. Williams, G.N. Parsons, Highly conductive and conformal poly(3,4-ethylenedioxythiophene) (PEDOT) thin films via oxidative molecular layer deposition, Chemistry of Materials 26 (2014) 3471–3478. https://doi.org/10.1021/cm500825b

[82] Q.K. Wyatt, M. Vaninger, N.C. Paranamana, T.W. Heitmann, H. Kaiser, M.J. Young, Oxidative molecular layer deposition of amine-containing conjugated polymer thin films, ACS Appl Polym Mater 4 (2022) 6156–6168. https://doi.org/10.1021/acsapm.2c00942

[83] D. Zacher, O. Shekhah, C. Wöll, R.A. Fischer, Thin films of metal–organic frameworks, Chem Soc Rev 38 (2009) 1418–1429. https://doi.org/10.1039/b805038b

[84] C. Crivello, S. Sevim, O. Graniel, C. Franco, S. Pane, J. Puigmarti-Luis, D. Munoz-Rojas, Advanced technologies for the fabrication of MOF thin films, Mater Horiz 8 (2021) 168–178. https://doi.org/10.1039/d0mh00898b

[85] O. Shekhah, J. Liu, R.A. Fischer, C. Wöll, MOF thin films: existing and future applications, Chem Soc Rev 40 (2011) 1081–1106. https://doi.org/10.1039/c0cs00147c

[86] J. Kint, F. Mattelaer, S. Sarah, T. Vandenbroucke, A. Muriqi, M.M. Minjauw, M. Nisula, P.M. Vereecken, M. Nolan, J. Dendooven, C. Detavernier, Molecular layer

deposition of " magnesicone ", a magnesium-based hybrid material, Chemistry of Materials 32 (2020) 4451–4466. https://doi.org/10.1021/acs.chemmater.9b05116.

[87] Q. Peng, B. Gong, R.M. VanGundy, G.N. Parsons, "Zincone" zinc oxide - organic hybrid polymer thin films formed by molecular layer deposition, Chemistry of Materials 21 (2009) 820–830. https://doi.org/10.1021/cm8020403

[88] A. Vázquez-López, A. Yaseen, D. Maestre, J. Ramírez-Castellanos, E.S. Marstein, S.Z. Karazhanov, A. Cremades, Synergetic improvement of stability and conductivity of hybrid composites formed by PEDOT:PSS and SnO nanoparticles, Molecules 25 (2020). https://doi.org/10.3390/molecules25030695

[89] A.J. Karttunen, T. Tynell, M. Karppinen, Atomic-level structural and electronic properties of hybrid inorganic-organic ZnO:Hydroquinone superlattices fabricated by ALD/MLD, Journal of Physical Chemistry C 119 (2015) 13105–13114. https://doi.org/10.1021/acs.jpcc.5b03433

[90] K.B. Klepper, O. Nilsen, S. Francis, H. Fjellvåg, Guidance of growth mode and structural character in organic-inorganic hybrid materials-a comparative study, Dalton Transactions 43 (2014) 3492–3500. https://doi.org/10.1039/c3dt52391h

[91] W. Al Zoubi, M.P. Kamil, S. Fatimah, N. Nashrah, Y.G. Ko, Recent advances in hybrid organic-inorganic materials with spatial architecture for state-of-the-art applications, Prog Mater Sci 112 (2020) 100663. https://doi.org/10.1016/j.pmatsci.2020.100663

[92] W. Xiao, D. Yu, S.F. Bo, Y.Y. Qiang, Y. Dan, C. Ping, D.Y. Hui, Z. Yi, The improvement of thin film barrier performances of organic-inorganic hybrid nanolaminates employing a low-temperature MLD/ALD method, RSC Adv 4 (2014) 43850–43856. https://doi.org/10.1039/c4ra06638c

[93] S.M. George, B.H. Lee, B. Yoon, A.I. Abdulagatov, R.A. Hall, Metalcones: Hybrid organic-inorganic films fabricated using atomic and molecular layer deposition techniques, J Nanosci Nanotechnol, 11 (2011) 7948–7955. https://doi.org/10.1166/jnn.2011.5034

[94] P. Sundberg, M. Karppinen, Organic-inorganic thin films from $TiCl_4$ and 4-aminophenol precursors: a model case of ALD/MLD hybrid-material growth?, Eur J Inorg Chem (2014) 968–974. https://doi.org/10.1002/ejic.201301560

[95] K.B. Klepper, O. Nilsen, H. Fjellvåg, Deposition of thin films of organic–inorganic hybrid materials based on aromatic carboxylic acids by atomic layer deposition, Dalton Transactions 39 (2010) 11628. https://doi.org/10.1039/c0dt00817f

[96] O. Nilsen, K.R. Haug, T. Finstad, Molecular hybrid structures by atomic layer deposition - deposition of Alq3, Znq2 and Tiq4 (q = 8-hydroxyquinoline), Chemical Vapor Deposition 19 (2013) 174–179. https://doi.org/10.1002/cvde.201207043

[97] B. Yoon, D. Seghete, A.S. Cavanagh, S.M. George, Molecular layer deposition of hybrid organic - Inorganic alucone polymer films using a three-step abc reaction sequence, Chemistry of Materials 21 (2009) 5365–5374. https://doi.org/10.1021/cm9013267

[98] K. Gregorczyk, M. Knez, Hybrid nanomaterials through molecular and atomic layer deposition: top down, bottom up, and in-between approaches to new materials, Prog Mater Sci 75 (2016) 1–37. https://doi.org/10.1016/j.pmatsci.2015.06.004

[99] M. S. Raven, Review radio frequency sputtering and the deposition of high-temperature superconductors. Journal of Material Science: Materials in Electronics 5 (1994) 129–146. https://doi.org/10.1007/BF01198944

[100] H. Biederman, S.M. Ojha, L. Holland, The properties of fluorocarbon films prepared by r.f. sputtering and plasma polymerization in inert and active gas, 41 (1977) 329–339. https://doi.org/10.1016/0040-6090(77)90319-4

[101] H. Biederman, Organic films prepared by polymer sputtering, Journal of Vacuum Science & Technology A: Vacuum, Surfaces, and Films 18 (2000) 1642–1648. https://doi.org/10.1116/1.582399

[102] R. Harrop, P.J. Harrop, Friction of sputtered PTFE films, Thin Solid Films 3 (1969) 109–117. https://doi.org/10.1016/0040-6090(69)90083-2106

[103] J.M. Tibbitt, M. Shen, A.T. Bell, A comparison of r.f. sputtered and plasma polymerized thin films of tetra-fluoroethylene, Thin Solid Films 29 (1975) L43-L45. https://doi.org/10.1016/0040-6090(75)90187-X

[104] H. Usui, Preparation of polymer thin films by physical vapor deposition, Functional Polymer Films, 1 (2011) 287–318. Wiley-VCH. https://doi.org/10.1002/9783527638482.ch9

[105] A. Baptista, F.J.G. Silva, J. Porteiro, J.L. Míguez, G. Pinto, L. Fernandes, On the physical vapour deposition (PVD): evolution of magnetron sputtering processes for industrial applications, Procedia Manuf, Elsevier B.V. (2018) 746–757. https://doi.org/10.1016/j.promfg.2018.10.125

[106] G. Srinivasan, N. Gopalakrishnan, Y.S. Yu, R. Kesavamoorthy, J. Kumar, Influence of post-deposition annealing on the structural and optical properties of ZnO thin films

prepared by sol-gel and spin-coating method, Superlattices Microstruct 43 (2008) 112–119. https://doi.org/10.1016/j.spmi.2007.07.032

[107] J.I. Lee, Y.D. Park, Improving molecular structure in polythiophene thin films by solvent dipping post-treatment, Mater Chem Phys 247 (2020) 122878. https://doi.org/10.1016/j.matchemphys.2020.122878

[108] S. Liu, H. Deng, Y. Zhao, S. Ren, Q. Fu, The optimization of thermoelectric properties in a PEDOT:PSS thin film through post-treatment, RSC Adv 5 (2015) 1910–1917. https://doi.org/10.1039/c4ra09147g

[109] A.M. Hiszpanski, Y.L. Loo, Directing the film structure of organic semiconductors via post-deposition processing for transistor and solar cell applications, Energy Environ Sci 7 (2014) 592–608. https://doi.org/10.1039/c3ee42615g

[110] A.M. Hiszpanski, R.M. Baur, B. Kim, N.J. Tremblay, C. Nuckolls, A.R. Woll, Y.L. Loo, Tuning polymorphism and orientation in organic semiconductor thin films via post-deposition processing, J Am Chem Soc 136 (2014) 15749–15756. https://doi.org/10.1021/ja5091035

[111] A.M. Hiszpanski, S.S. Lee, H. Wang, A.R. Woll, C. Nuckolls, Y.L. Loo, Post-deposition processing methods to induce preferential orientation in contorted hexabenzocoronene thin films, ACS Nano 7 (2013) 294–300. https://doi.org/10.1021/nn304003u

[112] W.C. Tsoi, D.T. James, E.B. Domingo, J.S. Kim, M. Al-Hashimi, C.E. Murphy, N. Stingelin, M. Heeney, J.S. Kim, Effects of a heavy atom on molecular order and morphology in conjugated polymer:fullerene photovoltaic blend thin films and devices, ACS Nano 6 (2012) 9646–9656. https://doi.org/10.1021/nn304024g

[113] H. Shi, C. Liu, Q. Jiang, J. Xu, Effective approaches to improve the electrical conductivity of PEDOT:PSS: a review, Adv Electron Mater 1 (2015) 1500017. https://doi.org/10.1002/aelm.201500017

[114] Y.H. Lee, J. Oh, S.S. Lee, H. Kim, J.G. Son, Highly ordered nanoconfinement effect from evaporation-induced self-assembly of block copolymers on in situ polymerized PEDOT:Tos, ACS Macro Lett 6 (2017) 386–392. https://doi.org/10.1021/acsmacrolett.7b00137

[115] Q. Li, J. Yang, S. Chen, J. Zou, W. Xie, X. Zeng, Highly conductive PEDOT:PSS transparent hole transporting layer with solvent treatment for high performance silicon/organic hybrid solar cells, Nanoscale Res Lett 12 (2017) 506. https://doi.org/10.1186/s11671-017-2276-5

[116] M.N. Gueye, A. Carella, N. Massonnet, E. Yvenou, S. Brenet, J. Faure-Vincent, S. Pouget, F. Rieutord, H. Okuno, A. Benayad, R. Demadrille, J.P. Simonato, Structure and dopant engineering in PEDOT thin films: Practical tools for a dramatic conductivity enhancement, Chemistry of Materials 28 (2016) 3462–3468. https://doi.org/10.1021/acs.chemmater.6b01035

[117] J. Alam, X. Xu, P.C.O. Adu, Q. Meng, K. Zuber, S. Afshar, H.-C. Kuan, J. Ma, Enhancing thermoelectric performance of PEDOT: PSS: a review of treatment and nanocomposite strategies, Advanced Nanocomposites 1 (2024) 16–38. https://doi.org/10.1016/j.adna.2023.08.001

[118] Y. Xia, K. Sun, J. Ouyang, Solution-processed metallic conducting polymer films as transparent electrode of optoelectronic devices, Advanced Materials 24 (2012) 2436–2440. https://doi.org/10.1002/adma.201104795

[119] N. Kim, S. Kee, S.H. Lee, B.H. Lee, Y.H. Kahng, Y.R. Jo, B.J. Kim, K. Lee, Highly conductive PEDOT:PSS nanofibrils induced by solution-processed crystallization, Advanced Materials 26 (2014) 2268–2272. https://doi.org/10.1002/adma.201304611

[120] S.R.S. Kumar, N. Kurra, H.N. Alshareef, Enhanced high temperature thermoelectric response of sulphuric acid treated conducting polymer thin films, J Mater Chem C Mater 4 (2015) 215–221. https://doi.org/10.1039/c5tc03145a

[121] X. Wang, A.K.K. Kyaw, C. Yin, F. Wang, Q. Zhu, T. Tang, P.I. Yee, J. Xu, Enhancement of thermoelectric performance of PEDOT:PSS films by post-treatment with a superacid, RSC Adv 8 (2018) 18334–18340. https://doi.org/10.1039/c8ra02058b

[122] L. Bießmann, N. Saxena, N. Hohn, M.A. Hossain, J.G.C. Veinot, P. Müller-Buschbaum, Highly conducting, transparent PEDOT:PSS polymer electrodes from post-treatment with weak and strong acids, Adv Electron Mater 5 (2019). https://doi.org/10.1002/aelm.201800654

[123] J. Song, G. Ma, F. Qin, L. Hu, B. Luo, T. Liu, X. Yin, Z. Su, Z. Zeng, Y. Jiang, G. Wang, Z. Li, High-conductivity, flexible and transparent PEDOT: PSS electrodes for high performance semi-transparent supercapacitors, Polymers (Basel) 12 (2020). https://doi.org/10.3390/polym12020450

[124] Y. Shi, Y. Zhou, R. Shen, F. Liu, Y. Zhou, Solution-based synthesis of PEDOT:PSS films with electrical conductivity over 6300 S/cm, Journal of Industrial and Engineering Chemistry 101 (2021) 414–422. https://doi.org/10.1016/j.jiec.2021.05.036

[125] M.Z. Ali, K.M. Ku Ishak, M.A. Md Zawawi, Z. Zulkifli, M. Jaafar, Z. Ahmad, Single-step treatment to improve conductivity of PEDOT:PSS by hydrobromic acid solution for application of transparent electrode, Org Electron 110 (2022) 106643. https://doi.org/10.1016/j.orgel.2022.106643

[126] S. Khasim, A. Pasha, M. Lakshmi, P. Chellasamy, M. Kadarkarai, A.A.A. Darwish, T.A. Hamdalla, S.A. Al-Ghamdi, S. Alfadhli, Post treated PEDOT-PSS films with excellent conductivity and optical properties as multifunctional flexible electrodes for possible optoelectronic and energy storage applications, Opt Mater (Amst) 125 (2022). https://doi.org/10.1016/j.optmat.2022.112109

[127] J. Holopainen, M. Ritala, Rapid production of bioactive hydroxyapatite fibers via electroblowing, J Eur Ceram Soc 36 (2016) 3219–3224. https://doi.org/10.1016/j.jeurceramsoc.2016.05.011

[128] K.E. Aasmundtveit, E.J. Samuelsen, L.A.A. Pettersson, O. Inganäs, T. Johansson, R. Feidenhans'l, Structure of thin films of poly(3,4-ethylenedioxythiophene), Synth Met 101 (1999) 561–564. https://doi.org/10.1016/S0379-6779(98)00315-4

[129] T.I. Dyuzheva, N.A. Bendeliani, A.N. Glushko, S.S. Kabalkina, Phase diagram of ReO_3 up to 10 GPa, Phys Scr 39 (1989) 341–342. https://doi.org/10.1088/0031-8949/39/3/013

[130] A.M. Seligman, M.J. Karnovsky, H.L. Wasserkrug, J.S. Hanker, Nondroplet ultrastructural demonstration of cytochrome oxidase activity with a polymerizing osmiophilic reagent, diaminobenzidine (DAB)., J Cell Biol 38 (1968) 1–14. https://doi.org/10.1083/jcb.38.1.1

[131] K. Sakaino, Y. Kawabata, S. Adachiz, Etching characteristics of si(100) surfaces in an aqueous NaOH solution, J Electrochem Soc 147 (2000) 1530. https://doi.org/10.1149/1.1393389

[132] A.N. Hammoud, J.L. Suthar, Characterization of polybenzimidazole (PBI) film at high temperatures, Conference Record of IEEE International Symposium on Electrical Insulation (1992) 449–451. https://doi.org/10.1109/elinsl.1990.109793

[133] P.J. Rezlcroft, H. Scott, P.L. Kv-Onicky, F.L. Serdjin, The effect of high energy radiation on the electrical characteristics of pyrrone polymers, Journal of Applied Polymer Science 14 (1970) 1361–1372. https://doi.org/10.1002/app.1970.070140520

[134] P.J. Reucroft, H. Scott, F.L. Serafin, Photoconducting pyrrone polymers, Journal of Polymer Science Part C: Polymer Symposia 3 (1970) 261–269. https://doi.org/10.1002/polc.5070300129